J. Fluid Mech. (2018), *vol.* 851, *pp.* 447–478.
doi:10.1017/jfm.2018.492

Correlation coefficients of thermodynamic fluctuations in compressible aerodynamic turbulence

G. A. Gerolymos[1] and I. Vallet[1,†]

[1]Sorbonne Université, Faculty of Science and Engineering, 4 place Jussieu, 75005 Paris, France

(Received 17 October 2017; revised 13 April 2018; accepted 11 June 2018;
first published online 25 July 2018)

Thermodynamic fluctuations of pressure, density, temperature or entropy $\{p', \rho', T', s'\}$ in compressible aerodynamic turbulence, although generated by the flow, are fundamentally related to one another by the thermodynamic equation of state. Ratios between non-dimensional root-mean-square (r.m.s.) levels ($\mathrm{CV}_{p'} := \bar{p}^{-1} p'_{rms}$, $\mathrm{CV}_{\rho'} := \bar{\rho}^{-1} \rho'_{rms}$, $\mathrm{CV}_{T'} := \bar{T}^{-1} T'_{rms}$), along with all possible 2-moment correlation coefficients $\{c_{\rho'T'}, c_{p'\rho'}, c_{p'T'}, c_{s'\rho'}, c_{s'T'}, c_{s'p'}\}$, represent, in the sense of Bradshaw (*Annu. Rev. Fluid Mech.*, vol. 9, 1977, pp. 33–54), the thermodynamic turbulence structure of the flow. We use direct numerical simulation (DNS) data, both for plane channel flow and for sustained homogeneous isotropic turbulence, to determine the range of validity of the leading-order, formally $O(\mathrm{CV}_{\rho'})$, approximations of the exact relations between thermodynamic turbulence structure parameters. Available DNS data are mapped on the $(\mathrm{CV}_{\rho'}^{-1}\mathrm{CV}_{T'}, c_{\rho'T'})$-plane and their loci, identified using the leading-order approximations, highlight specific behaviour for different flows or flow regions. For the particular case of sustained compressible homogeneous isotropic turbulence, it is shown that the DNS data collapse onto a single curve corresponding to $c_{s'T'} \approxeq 0.2$ (for air flow), while the approximation $c_{s'p'} \approxeq 0$ fits reasonably well wall turbulence DNS data, providing building blocks towards the construction of simple phenomenological models.

Key words: compressible boundary layers, turbulence theory, turbulent flows

1. Introduction

We study the behaviour of thermodynamic fluctuations in compressible aerodynamic turbulence. It is well known (Hansen 1958, figure 1, p. 57) that, for temperatures $T \lessapprox$ 2000 K, the equation of state of air flow can be reasonably approximated by the so-called perfect-gas equation of state (Liepmann & Roshko 1957, § 1, pp. 1–37)

$$\mathcal{Z}(\rho, T) := \frac{p}{\rho R_g T} = 1 \iff p = \rho R_g T \implies \begin{cases} a = \sqrt{\gamma(T)\, R_g T} \\ \gamma(T) := \dfrac{c_p(T)}{c_v(T)} = \dfrac{c_p(T)}{c_p(T) - R_g}, \end{cases} \tag{1.1}$$

† Email address for correspondence: isabelle.vallet@upmc.fr

where $R_g = \text{const.}$ is the gas constant ($R_g = 287.04$ m^2 s^{-2} K^{-1} for air), p is the pressure, ρ is the density, T is the temperature, $\mathcal{Z}$ is the compressibility factor (Hansen 1958, p. 7), $c_p(T)$ and $c_v(T) = c_p(T) - R_g$ are the specific heats at constant pressure or volume, with ratio $\gamma(T)$, and $a(T)$ is the sound speed. At higher temperatures, dissociation of oxygen is the first phenomenon causing departure from (1.1), this departure occurring at higher temperatures with increasing pressure (Hansen 1958, figure 1, p. 57). Throughout the paper, the validity of (1.1) is assumed, and its implications for thermodynamic fluctuations in compressible turbulent flows are studied.

Standard decomposition $(\cdot) = \overline{(\cdot)} + (\cdot)'$ (Huang, Coleman & Bradshaw 1995, (2.1), p. 188) in Reynolds (ensemble) averages $\overline{(\cdot)}$ and fluctuations $(\cdot)'$ is used in the paper, for any flow quantity $(\cdot)$. An initial attempt to use Favre (mass-weighted) decomposition, $(\cdot) = \widetilde{(\cdot)} + (\cdot)''$, for T and s, as is generally the case for transport equations (Gerolymos & Vallet 2014), was inconclusive, both because it did not offer any particular conciseness in the relations between thermodynamic fluctuations and because it presents some mathematical difficulties in defining coefficients of variation and correlation coefficients in a strict mathematical sense. Furthermore, the correlation coefficient $c_{\rho' T'}$ comes out as an important parameter in the present work, independently of the relative importance of $\overline{T''} = -c_{\rho' T'}\,\mathrm{CV}_{\rho'}\,\mathrm{CV}_{T'}\,\bar{T}$.

The intensity of the fluctuations of thermodynamic state variables (p, ρ, T) is quantified by their coefficients of variation ($\mathrm{CV}_{\rho'} := \bar{\rho}^{-1}\rho'_{rms}$, $\mathrm{CV}_{T'} := \bar{T}^{-1}T'_{rms}$, $\mathrm{CV}_{p'} := \bar{p}^{-1}p'_{rms}$) i.e. their relative r.m.s. (root-mean-square) fluctuation levels (§ 2.1). The perfect-gas equation of state (1.1) implies exact nonlinear relations between coefficients of variation of the state variables and correlation coefficients between thermodynamic fluctuations. Such relations are of general validity, independently of the particular flow that is investigated. Thermodynamic relations based on the linearized truncation $\bar{p}^{-1}p' \cong \bar{\rho}^{-1}\rho' + \bar{T}^{-1}T'$ (Gatski & Bonnet 2009, (3.114), p. 72) of the exact expansion of (1.1) are widely used (Kovásznay 1953; Taulbee & VanOsdol 1991): this approach studies compressible turbulence in the limiting case of small relative fluctuation amplitudes, neglecting quadratic or higher-order terms. The point should be made, nonetheless, that the assumption that the relative r.m.s.-levels, $\bar{\rho}^{-1}\rho'_{rms}$ and $\bar{T}^{-1}T'_{rms}$, are small, which is used in some parts of the paper, is less stringent than assuming that the instantaneous levels, $\bar{\rho}^{-1}\rho'$ and $\bar{T}^{-1}T'$ are invariably small, as in the standard linearized approximation (Gatski & Bonnet 2009, (3.114), p. 72). Mahesh, Lele & Moin (1997) use, in the context of the Reynolds analogy assumptions (Morkovin 1962), the term 'weak form' for relations in a r.m.s. sense, as opposed to 'strong form' for instantaneous relations. This point is further is highlighted in Barre & Bonnet (2015) who distinguish between the SRA (strong Reynolds analogy) involving relations between variances and covariances and the VSRA (very strong Reynolds analogy) invoking instantaneous fluctuating relations. The acoustic, vorticity and entropy modes describing the essential dynamics of compressible turbulence (Kovásznay 1953) are the mathematical result of linearized analysis. However, the higher-order (nonlinear) coupling between modes identified from the general small-perturbation series expansion of the compressible Navier–Stokes equations (Chu & Kovásznay 1958) is essential in completing this now classic view of gas dynamic turbulence. Nonetheless, Blaisdell, Mansour & Reynolds (1993) point out the difficulty of using this approach 'to study fully nonlinear turbulence for which the decomposition into such modes cannot be made'.

Often, in studies of compressible turbulence, some representative Mach number is assumed to quantify compressibility effects (Smits & Dussauge 2006, § 4.5,

pp. 105–108), e.g. the turbulent Mach number M_T (Gatski & Bonnet 2009, (5.1), p. 118), which is essentially (Blaisdell *et al.* 1993, p. 454) approximately equal to M'_{rms} (provided $\mathrm{CV}_{T'}$ is sufficiently small), or the gradient Mach number M_g (Smits & Dussauge 2006, p. 107), introduced by Sarkar (1995). The widespread use of such scalings should be attributed to the deliberate choice of attempting to relate compressibility effects on turbulence to parameters of the dynamic (velocity $\bar{u}_i + u'_i$) field. Correlations based on these local turbulence-representative Mach numbers lack universality, in the sense that their applicability is flow dependent. On the contrary, Morkovin's (1962) ideas on the effects of compressibility on turbulence, directly point to $\mathrm{CV}_{\rho'}$ as the primary indicator, a fact explicitly formulated by Bradshaw (1977).

The idea that thermodynamic turbulence i.e. $\{p', \rho', T', s'\}$ is subordinate to the dynamic field $\{\bar{u}_i, u'_i\}$ is central in compressible-turbulence research. There are numerous examples of this approach, e.g. various parametrizations in terms of M_T (Donzis & Jagannathan 2013) or M_g (Sarkar 1995), but also the various forms of Reynolds analogy (Huang *et al.* 1995; Guarini *et al.* 2000; Zhang *et al.* 2013) relating shear-flow temperature transport $\overline{T'v'}$ to momentum transport $\overline{u'v'}$. The underlying assumption of all these approaches is that p' is essentially a consequence of the velocity field $\{\bar{u}_i, u'_i\}$, through the compressible-flow Poisson equation (Gerolymos, Sénéchal & Vallet 2013, (A 1e), p. 46). To leading order in $\mathrm{CV}_{\rho'}$ (Foysi, Sarkar & Friedrich 2004), the source terms of this Poisson equation are the basic incompressible mechanisms (Kim 1989, slow, rapid and Stokes), with variable $\bar{\rho}$ and $\bar{T}$ to account for mean-flow stratification, in the sense of Morkovin's (1962) hypothesis. Beyond this regime, when $\mathrm{CV}_{\rho'}$ is high, several other source terms in the Poisson equation for p', representing compressible-turbulence (ρ') mechanisms may become important (Foysi *et al.* 2004), including the wave-like term (Pantano & Sarkar 2002): coupling between p' and ρ' becomes important. Notice also, that the p'-Hessian is governed, in compressible flow, by a specific transport equation (Suman & Girimaji 2001, (2.9), p. 292), involving ρ'-dependent terms.

The particular approach of compressible-turbulence analysis notwithstanding, thermodynamic fluctuations are interrelated by the equation of state (1.1) and its basic thermodynamic (Liepmann & Roshko 1957, § 1, pp. 1–37) consequences (1.1). There are, however, few studies concentrating on these relations. Donzis & Jagannathan (2013) have investigated in detail the behaviour of thermodynamic fluctuations $\{p', \rho', T'\}$ in sustained compressible homogenous isotropic turbulence (HIT), including the $c_{\rho'T'}$ correlation coefficient, skewness, flatness and p.d.f.s (probability density functions). This study (Donzis & Jagannathan 2013) highlights the influence of compressibility $\mathrm{CV}_{\rho'}$, p.d.f.s tending to near-Gaussian values for skewness and flatness with increasing M_T implying increasing $\mathrm{CV}_{\rho'}$. Gerolymos & Vallet (2014) have studied, for compressible plane channel flow, the budgets of the transport equations for the variances and fluxes of the thermodynamic fluctuations $\{p', \rho', T', s'\}$, and provided data for correlation coefficients between thermodynamic fluctuations (Gerolymos & Vallet 2014, figure 7, p. 723). Wei & Pollard (2011, figure 1, p. 6) suggest that the correlation coefficient $c_{p'\rho'}$ decreases near the wall with increasing Mach number, but its level is probably also Re-dependent (Gerolymos & Vallet 2014). Several authors (Lechner, Sesterhenn & Friedrich 2001; Shadloo, Hadjadj & Hussain 2015) have used two-dimensional (2-D) scatter plots of relative amplitudes to gain insight into the correlation between thermodynamic fluctuations. Duan, Choudhari & Zhang (2016) studied using direct numerical simulation (DNS) 2-point/2-time p'-correlations in a hypersonic $\bar{M}_e \approxeq 5.86$ cold-wall boundary layer and obtained detailed information on the convective velocity of p' in the boundary layer and on the acoustic field radiated in the free stream.

In the absence of direct p' measurements, early shear-flow hot-wire practice (Kovásznay 1953; Kistler 1959; Morkovin 1962), assumed that in supersonic ($\bar{M}_e \lessapprox 5$) boundary layers $\mathrm{CV}_{p'} \ll \mathrm{CV}_{\rho'} = O(\mathrm{CV}_{T'})$, expecting (Morkovin 1962) that $\mathrm{CV}_{p'}$ would become important only at higher external flow Mach number $\bar{M}_e$. Of course DNS data (Coleman, Kim & Moser 1995) largely moderate this assumption, since near the wall, although $\mathrm{CV}_{p'} < \mathrm{CV}_{\rho'}$, they both are still of the same order of magnitude (Gerolymos & Vallet 2014), while further away from the wall (wake region) $\mathrm{CV}_{p'} > \mathrm{CV}_{\rho'}$. Laderman & Demetriades (1974) were probably the first to make an approximate assessment of $\mathrm{CV}_{p'}$ in their analysis of $\bar{M}_e \cong 9.4$ boundary-layer measurements: interestingly they assumed that p' and s' were uncorrelated (Laderman & Demetriades 1974, $c_{s'p'} = 0$; table 2, p. 138). This assumption is approximately verified by recent wall turbulence DNS data (Gerolymos & Vallet 2014, figure 7, p. 723). Barre & Bonnet (2015), citing Blaisdell *et al.* (1993), associate the approximation $c_{s'p'} = 0$ with the decoupling of acoustic and entropy modes in supersonic turbulence (Kovásznay 1953). On the other hand, Pantano & Sarkar (2002, pp. 351–352) using the thermodynamic identity $D_t p = (\partial_\rho p)_s D_t\rho + (\partial_s p)_\rho D_t s$ assumed that *ps*-coupling becomes dominant as the convective Mach number M_c increases.

Contrary to studies of astrophysical turbulence, where a tentative thermodynamic model is constructed assuming explicitly isothermal or polytropic behaviour (Banerjee & Galtier 2014), in aerodynamic (more generally gas dynamic) flows the working medium thermodynamics is known, and the weakly compressible regime or the quasi-incompressible limit are the consequences of the characteristic flow Mach number $M_{ref} \to 0$. In modelling work, Rubesin (1976, (47), p.10) introduces the assumption of polytropic behaviour of thermodynamic fluctuations, with polytropic exponent n_P which can be considered a modelling parameter (flow dependent). This polytropic behaviour can also be considered in an r.m.s.-sense (Barre & Bonnet 2015). Notice that analysis of plane-mixing-layer DNS data at convective Mach number $M_c = 1$ clearly indicate that free shear turbulence is not polytropic (Barre & Bonnet 2015, figure 13, p. 331).

The above cited references explicitly study thermodynamic fluctuations and their correlations. We do not include here many other studies on the dynamic field in compressible turbulence, which are reviewed elsewhere (Lele 1994; Guarini *et al.* 2000; Duan & Martín 2011; Lagha *et al.* 2011; Zhang *et al.* 2013; Gerolymos & Vallet 2014; Modesti & Pirozzoli 2016). Phenomenological models such as eddy-shocklets (Lee, Lele & Moin 1991), pseudo-sound (Ristorcelli 1997) and compressibility damping of the velocity/pressure-gradient correlation (Sarkar 1995; Pantano & Sarkar 2002) have evolved to explain the effects of compressibility on turbulence dynamics.

The paper focuses on the relations between thermodynamic fluctuations $\{p', \rho', T', s'\}$ implied by (1.1). Compressibility $\mathrm{CV}_{\rho'}$ principally controls the level of thermodynamic fluctuations $\{\mathrm{CV}_{p'}, \mathrm{CV}_{\rho'}, \mathrm{CV}_{T'}\}$. On the other hand, the set of ratios of these relative levels, along with all possible 2-moment correlation coefficients

$$\mathrm{TTS} := \left\{ \frac{\mathrm{CV}_{T'}}{\mathrm{CV}_{\rho'}}, \frac{\mathrm{CV}_{p'}}{\mathrm{CV}_{\rho'}}, \frac{s'_{rms}}{R_g \mathrm{CV}_{\rho'}}, c_{\rho'T'}, c_{p'\rho'}, c_{p'T'}, c_{s'\rho'}, c_{s'T'}, c_{s'p'} \right\} \tag{1.2}$$

defines, in the sense of Bradshaw (1977), the thermodynamic turbulence structure of the flow. The analysis of DNS data will show that, although weakly (slowly) dependent on the characteristic Mach number of the flow, the set TTS (1.2) is rather the footprint of the specific type of flow. Furthermore, for weakly compressible

turbulence ($\mathrm{CV}_{\rho'} \ll 1$) the knowledge of any couple of elements of TTS suffices to determine to $O(\mathrm{CV}_{\rho'})$ all the other elements. We use the $(\mathrm{CV}_{\rho'}^{-1}\,\mathrm{CV}_{T'}, c_{\rho'T'})$-plane to map the behaviour of thermodynamic turbulence of various flows.

In § 2 we introduce notation, summarize exact relations and expansions of various terms in the set TTS (1.2). In (§ 3) we examine the relative magnitude of the coefficients of variation of thermodynamic variables ($\mathrm{CV}_{\rho'}$, $\mathrm{CV}_{T'}$, $\mathrm{CV}_{p'}$) obtained from DNS both of sustained solenoidally forced compressible homogeneous isotropic turbulence (§ 3.1) and of compressible turbulent plane channel flow (§ 3.2). In § 4 we study approximate (leading-order) relations between correlation coefficients and coefficients of variation, at the limit of weakly compressible turbulence, defined by the condition $\mathrm{CV}_{\rho'} \ll 1$. These approximations and their leading error are evaluated against DNS data (§ 5) to assess their range of validity and robustness. In § 6 we map compressible turbulence on a plane defined by two structure parameters, revealing consistent behaviour of DNS data for different types of flow or regions of flow, which is identified using the leading-order relations (§ 4). In § 7 we use this observed behaviour of thermodynamic turbulence to develop phenomenological approximations of the elements of the set TTS (1.2) specific to the flows studied in § 6. Finally, in § 8 we summarize the main conclusions of the present work and discuss future perspectives.

2. Thermodynamic fluctuations and correlations

The fluctuating form of the equation of state (§ 2.3) implies exact relations between the relative r.m.s. magnitudes (§ 2.1) and the correlation coefficients (§ 2.2) of the thermodynamic fluctuations $\{p', \rho', T'\}$. Entropy can be expanded in a power series of $\{p', \rho', T'\}$ (§ 2.4).

2.1. *Coefficients of variation*

The coefficient of variation of a flow quantity is (Pham 2006, (48.1), p. 906) the r.m.s. of the relative fluctuation, i.e.

$$\mathrm{CV}_{(\cdot)'} := \frac{\sqrt{\overline{(\cdot)'^2}}}{\overline{(\cdot)}} = \left[\frac{(\cdot)'}{\overline{(\cdot)}}\right]_{rms} \tag{2.1a}$$

so that, in particular,

$$\mathrm{CV}_{\rho'} := \frac{\sqrt{\overline{\rho'^2}}}{\bar{\rho}} = \frac{\rho'_{rms}}{\bar{\rho}}; \quad \mathrm{CV}_{T'} := \frac{\sqrt{\overline{T'^2}}}{\bar{T}} = \frac{T'_{rms}}{\bar{T}}; \quad \mathrm{CV}_{p'} := \frac{\sqrt{\overline{p'^2}}}{\bar{p}} = \frac{p'_{rms}}{\bar{p}}. \tag{2.1b–d}$$

Although definitions (2.1) are not in general use, their introduction greatly simplifies notation in the equations developed in the paper. An important observation from available compressible DNS data (Donzis & Jagannathan 2013; Gerolymos & Vallet 2014; Jagannathan & Donzis 2016) is that, generally,

$$O\Bigg(\underbrace{\frac{\sqrt{\overline{T'^2}}}{\bar{T}}}_{\mathrm{CV}_{T'}}\Bigg) = O\Bigg(\underbrace{\frac{\sqrt{\overline{\rho'^2}}}{\bar{\rho}}}_{\mathrm{CV}_{\rho'}}\Bigg) = O\Bigg(\underbrace{\frac{\sqrt{\overline{p'^2}}}{\bar{p}}}_{\mathrm{CV}_{p'}}\Bigg) = O\Bigg(\underbrace{\frac{\sqrt{\overline{s'^2}}}{R_g}}_{R_g^{-1}s'_{rms}}\Bigg). \tag{2.2}$$

The last term in (2.2) represents the non-dimensional level of entropy fluctuations (§ 2.5), which was shown in Gerolymos & Vallet (2014, figure 5, p. 720) to be of the same order of magnitude and to follow a similar $\bar{M}_{CL}$-dependency as $\{\mathrm{CV}_{p'}, \mathrm{CV}_{\rho'}, \mathrm{CV}_{T'}\}$.

Condition (2.2) is central in the asymptotic expansions worked out in the paper. In weakly compressible turbulence, the defining assumption $\mathrm{CV}_{\rho'} \ll 1$ (Bradshaw 1977) is directly extended to the other thermodynamic variables by (2.2).

2.2. *Correlation coefficients*

The correlation coefficient (CC) between any 2 flow quantities $[\cdot]$ and $(\cdot)$ is defined by

$$c_{(\cdot)'[\cdot]'} := \frac{\overline{(\cdot)'[\cdot]'}}{\sqrt{\overline{(\cdot)'^2}}\sqrt{\overline{[\cdot]'^2}}} \in [-1, 1]. \tag{2.3a}$$

These correlation coefficients pertain to the 2-momenta between fluctuating quantities. Definition (2.3*a*) can be extended to higher-order correlations as

$$c_{(\cdot)'\cdots[\cdot]'} := \frac{\overline{(\cdot)'\cdots[\cdot]'}}{\sqrt{\overline{(\cdot)'^2}}\cdots\sqrt{\overline{[\cdot]'^2}}}. \tag{2.3b}$$

However, in the multiple correlation case, the correlation coefficient (nCC, $n \geqslant 3$) is not limited in a particular interval, unlike the 2-moment case (2.3*a*). Notice that by (2.3*b*) skewness and flatness are

$$S_{(\cdot)'} := \frac{\overline{(\cdot)'^3}}{\left[\sqrt{\overline{(\cdot)'^2}}\right]^3} \overset{(2.3b)}{=} c_{(\cdot)'(\cdot)'(\cdot)'}; \quad F_{(\cdot)'} := \frac{\overline{(\cdot)'^4}}{\left[\sqrt{\overline{(\cdot)'^2}}\right]^4} \overset{(2.3b)}{=} c_{(\cdot)'(\cdot)'(\cdot)'(\cdot)'}. \tag{2.3c,d}$$

2.3. *Fluctuating equation of state and correlations*

The basic thermodynamic variables (p, ρ, T) are related by the equation of state (1.1), implying

$$(1.1) \overset{(2.3)}{\Longrightarrow} \begin{cases} \bar{p} = \bar{\rho} R_g \bar{T}(1 + c_{\rho'T'}\,\mathrm{CV}_{\rho'}\,\mathrm{CV}_{T'}) \\ (1 + c_{\rho'T'}\,\mathrm{CV}_{\rho'}\,\mathrm{CV}_{T'})\dfrac{p'}{\bar{p}} = \dfrac{\rho'}{\bar{\rho}} + \dfrac{T'}{\bar{T}} + \dfrac{\rho'T'}{\bar{\rho}\bar{T}} - c_{\rho'T'}\,\mathrm{CV}_{\rho'}\,\mathrm{CV}_{T'}. \end{cases} \tag{2.4}$$

Often, approximations for weakly compressible turbulence are constructed directly from (2.4), by dropping all nonlinear terms (i.e. $\rho'T'$ and $\mathrm{CV}_{\rho'}\,\mathrm{CV}_{T'}$). It is nonetheless useful to consider a more systematic approach based on exact relations between correlation coefficients. Multiplying (2.4) by p', ρ' or T', we obtain, upon averaging the exact relations,

$$(1 + c_{\rho'T'}\,\mathrm{CV}_{\rho'}\,\mathrm{CV}_{T'})\mathrm{CV}_{p'} \overset{(2.4),\,(2.3)}{=} c_{p'\rho'}\,\mathrm{CV}_{\rho'} + c_{p'T'}\,\mathrm{CV}_{T'} + c_{p'\rho'T'}\,\mathrm{CV}_{\rho'}\,\mathrm{CV}_{T'} \tag{2.5a}$$

$$(1 + c_{\rho'T'}\,\mathrm{CV}_{\rho'}\,\mathrm{CV}_{T'})c_{p'\rho'}\mathrm{CV}_{p'} \overset{(2.4),\,(2.3)}{=} \mathrm{CV}_{\rho'} + c_{\rho'T'}\,\mathrm{CV}_{T'} + c_{\rho'\rho'T'}\,\mathrm{CV}_{\rho'}\,\mathrm{CV}_{T'} \tag{2.5b}$$

$$(1 + c_{\rho'T'}\,\mathrm{CV}_{\rho'}\,\mathrm{CV}_{T'})c_{p'T'}\mathrm{CV}_{p'} \overset{(2.4),\,(2.3)}{=} c_{\rho'T'}\,\mathrm{CV}_{\rho'} + \mathrm{CV}_{T'} + c_{\rho'T'T'}\,\mathrm{CV}_{\rho'}\,\mathrm{CV}_{T'}. \tag{2.5c}$$

2.4. *Entropy fluctuations*

For any bivariate substance, entropy, as a state variable, is defined (Liepmann & Roshko 1957, p. 338) by the differential equation

$$T\mathrm{d}s = \mathrm{d}h - \frac{\mathrm{d}p}{\rho} \overset{(1.1)}{\Longrightarrow} \begin{cases} \dfrac{\mathrm{d}s}{R_g} = \dfrac{c_p(T)}{R_g}\dfrac{\mathrm{d}T}{T} - \dfrac{\mathrm{d}p}{p} \\ = \dfrac{c_v(T)}{R_g}\dfrac{\mathrm{d}T}{T} - \dfrac{\mathrm{d}\rho}{\rho}. \end{cases} \tag{2.6}$$

Integrating (2.6) between the reference states $(\bar{p},\bar{T})$ or $(\bar{\rho},\bar{T})$ and the corresponding instantaneous turbulent flow conditions $(p,T)=(\bar{p}+p',\bar{T}+T')$ or $(\rho,T)=(\bar{\rho}+\rho',\bar{T}+T')$, respectively, readily yields

$$\frac{s-s_{(\bar{p},\bar{T})}}{R_g} \overset{(2.6)}{=} \frac{1}{R_g}\int_{\bar{T}}^{\bar{T}+T'} \frac{c_p(T^*)}{T^*}\,\mathrm{d}T^* - \ln\left(1+\frac{p'}{\bar{p}}\right), \tag{2.7a}$$

$$\frac{s-s_{(\bar{\rho},\bar{T})}}{R_g} \overset{(2.6)}{=} \frac{1}{R_g}\int_{\bar{T}}^{\bar{T}+T'} \frac{c_v(T^*)}{T^*}\,\mathrm{d}T^* - \ln\left(1+\frac{\rho'}{\bar{\rho}}\right), \tag{2.7b}$$

where we note $s_{(\bar{p},\bar{T})}$ and $s_{(\bar{\rho},\bar{T})}$ the entropy at the corresponding states, which are to $O(\mathrm{CV}^2_{\rho'})$ approximately equal to $\bar{s}$ (Lele 1994, p. 224). Relations (2.7) can be easily expanded in powers series of relative fluctuation amplitudes, and replacing $s=\bar{s}+s'$ we obtain the expansions for the entropy fluctuations, truncated after the quadratic terms

$$\begin{aligned} \frac{s'}{R_g} &\overset{(2.7a)}{\sim} \frac{\breve{\gamma}}{\breve{\gamma}-1}\left(\frac{T'}{\bar{T}} - \frac{1}{2}\left(\frac{T'}{\bar{T}}\right)^2\right) - \left(\frac{p'}{\bar{p}} - \frac{1}{2}\left(\frac{p'}{\bar{p}}\right)^2\right) + \frac{1}{2}\left(\frac{T'}{\bar{T}}\right)^2 \frac{\bar{T}}{R_g}\left.\frac{\mathrm{d}c_p}{\mathrm{d}T}\right|_{\bar{T}} \\ &\quad - \frac{\bar{s}-s_{(\bar{p},\bar{T})}}{R_g} + O\left(\left(\frac{p'}{\bar{p}}\right)^3, \left(\frac{T'}{\bar{T}}\right)^3\right) \end{aligned} \tag{2.8a}$$

$$\begin{aligned} &\overset{(2.7b)}{\sim} \frac{1}{\breve{\gamma}-1}\left(\frac{T'}{\bar{T}} - \frac{1}{2}\left(\frac{T'}{\bar{T}}\right)^2\right) - \left(\frac{\rho'}{\bar{\rho}} - \frac{1}{2}\left(\frac{\rho'}{\bar{\rho}}\right)^2\right) + \frac{1}{2}\left(\frac{T'}{\bar{T}}\right)^2 \frac{\bar{T}}{R_g}\left.\frac{\mathrm{d}c_p}{\mathrm{d}T}\right|_{\bar{T}} \\ &\quad - \frac{\bar{s}-s_{(\bar{\rho},\bar{T})}}{R_g} + O\left(\left(\frac{\rho'}{\bar{\rho}}\right)^3, \left(\frac{T'}{\bar{T}}\right)^3\right), \end{aligned} \tag{2.8b}$$

where we defined for brevity

$$\breve{\gamma} := \gamma(\bar{T}) \tag{2.8c}$$

following the convention that $\breve{\cdot}$ is a function of averaged quantities which cannot be identified with a Reynolds or Favre average (Gerolymos & Vallet 1996, 2014). Notice the presence of the constants $\bar{s}-s_{(\bar{p},\bar{T})}\neq 0\neq \bar{s}-s_{(\bar{\rho},\bar{T})}$, which are $O(\mathrm{CV}^2_{\rho'})$ (Lele 1994, p. 224), and are directly related to the nonlinearity of (2.7). The influence of variable $c_p(T)=R_g-c_v(T)$ (1.1) also induces a quadratic $O(\mathrm{CV}^2_{\rho'})$ term in the expressions for s' (2.8). Therefore, leading-order approximations related to s' are valid independently of the variability of $c_p(T)$, and depend only on the local value of $\gamma(\bar{T})$ (1.1). Notice that by (1.1) $d_T c_p = d_T c_v$.

2.5. *Entropy variance and correlations*

It is straightforward from (2.8) to calculate expansions for the entropy variance s'_{rms} and for correlation coefficients containing s'. Squaring and averaging (2.8*b*) and introducing definitions (2.1), (2.3) yields after simple calculations using (4.4), (A1)

$$\left(\frac{s'_{rms}}{R_g}\right)^2 \overset{(2.8b),\,(4.4),\,(A\,1),(2.2)}{\sim} \frac{\breve{\gamma}}{(\breve{\gamma}-1)^2}\,\mathrm{CV}^2_{T'} + \frac{\breve{\gamma}}{\breve{\gamma}-1}\,\mathrm{CV}^2_{\rho'} - \frac{1}{\breve{\gamma}-1}\,\mathrm{CV}^2_{p'} - \frac{\breve{\gamma}}{(\breve{\gamma}-1)^2}\,S_{T'}\,\mathrm{CV}^3_{T'} - \frac{\breve{\gamma}}{\breve{\gamma}-1}\,S_{\rho'}\,\mathrm{CV}^3_{\rho'} + \frac{1}{\breve{\gamma}-1}\,S_{p'}\,\mathrm{CV}^3_{p'} + c_{s'T'T'}\,\frac{s'_{rms}}{R_g}\,\mathrm{CV}^2_{T'}\,\frac{\bar{T}}{R_g}\,\frac{\mathrm{d}c_p}{\mathrm{d}T}\bigg|_{\bar{T}} + O(\mathrm{CV}^4_{\rho'}). \tag{2.9}$$

Notice that (2.9) implies that the correct non-dimensional expression for the entropy variance is $R_g^{-1}s'_{rms}$ and is of the same order of magnitude as the coefficients of variation of the basic thermodynamic quantities. The reason why $R_g^{-1}\,s'_{rms}$ should be considered in the order-of-magnitude relation (2.2) instead of $\mathrm{CV}_{s'}$ is because, by definition (2.6), entropy is defined with respect to an arbitrary reference state, so that the precise value of $\bar{s}$ that appears in the definition of $\mathrm{CV}_{s'}$ (2.1) has no physical significance: only entropy differences have physical meaning.

3. DNS data

The expansions and approximations developed in the paper are assessed against DNS data from two different aerodynamic configurations, viz sustained compressible HIT (Donzis & Jagannathan 2013, isotropic homogeneous turbulence) and fully developed compressible turbulent plane channel flow (Gerolymos & Vallet 2014). In both databases, the coefficient of variation of density $\mathrm{CV}_{\rho'}$ (2.1*b–d*) increases from very low values (which approach asymptotically the quasi-incompressible limit) to maximum values as high as 0.16 (figure 1). In both cases $\mathrm{CV}_{\rho'}$ varies with the representative Mach number, viz the turbulent Mach number M_T in HIT (3.1*a*) or the centreline Mach number $\bar{M}_{CL}$ in channel flow (3.2*a*).

Donzis & Jagannathan (2013, figure 2, p. 227) have estimated that in HIT $\mathrm{CV}_{\rho'}$ increases as $M_T^{2.2}$, the exponent being a best fit of the data. A slightly lower exponent of 2.1 also fits well the DNS data (figure 1). The channel DNS data (Gerolymos & Vallet 2014) indicate that $\mathrm{CV}_{\rho'}$ varies as $\bar{M}_{CL}^{2.1}$ (figure 1). The channel data fit very closely the $\bar{M}_{CL}^{2.1}$ variation both at the maximum near-wall peak and at the channel centreline, but exhibit some scatter at the wall. This is attributed to a $Re_{\tau^\star}$-influence, associated with the strictly isothermal wall boundary condition, which implies (Gerolymos & Vallet 2014, (3.5), p. 719) $[p'_{rms}]_w = a_w^2[\rho'_{rms}]_w \Longleftrightarrow [\mathrm{CV}_{p'}]_w = \gamma_w[\mathrm{CV}_{\rho'}]_w$; therefore, $[\mathrm{CV}_{\rho'}]_w$ follows the well known from incompressible channel flow (Tsuji *et al.* 2007) $Re_{\tau^\star}$-dependence of $[p'_{rms}]^+_w$.

As a conclusion, aerodynamic ($\gamma = 1.4$) DNS data indicate that $\mathrm{CV}_{\rho'}$ values for a given configuration, vary, at constant Re-number, proportionally to a power of the representative Mach number, with exponent $\in [2.1, 2.2]$, i.e. slightly higher than 2.

3.1. *Sustained compressible HIT*

Donzis & Jagannathan (2013) and Jagannathan & Donzis (2016) have performed DNS of sustained compressible HIT with solenoidal forcing at the large scales (Eswaran

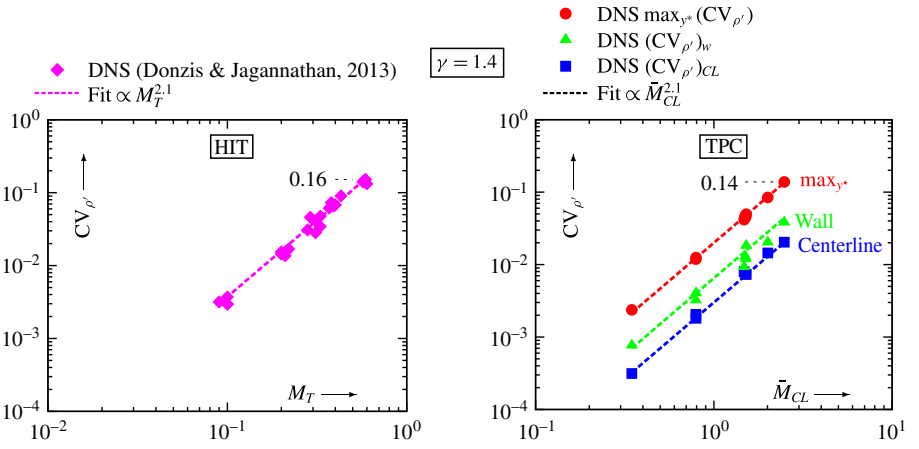

FIGURE 1. (Colour online) Log scale plots of DNS data, for the evolution of $\mathrm{CV}_{\rho'}$ versus $M_T \in [0.1, 0.6]$ in sustained homogeneous isotropic turbulence (HIT) simulations (Donzis & Jagannathan 2013; D. A. Donzis, 2016 Compressible HIT DNS data, Private communication, donzis@tamu.edu; Jagannathan & Donzis 2016), and for the evolution of $\mathrm{CV}_{\rho'}$ versus $\bar{M}_{CL} \in [0.3, 2.5]$ in fully developed compressible turbulent plane channel (TPC) flow (Gerolymos & Vallet 2014) at three different locations across the channel (wall, centreline and maximum value).

& Pope 1988). The flow is modelled by the compressible Navier–Stokes equations (Jagannathan & Donzis 2016, (3.1–3.5), p. 673), without bulk viscosity $\mu_b = 0$ (Gerolymos & Vallet 2014, (2.1e), p. 706), a power law for the dynamic viscosity $\mu(T) \propto \sqrt{T}$ and constant Prandtl number $Pr = 0.72$ (Donzis & Jagannathan 2013, p. 224). The working medium follows the equation of state (1.1) with a constant ratio of specific heats (1.1) $\gamma = 1.4$ (Donzis & Jagannathan 2013, figure 7, p. 234). The representative parameters in this configuration are the turbulent Mach number M_T (Jagannathan & Donzis 2016, p. 670) and the Taylor-microscale Reynolds number Re_λ (Jagannathan & Donzis 2016, p. 671)

$$M_T := \frac{\sqrt{\overline{u_i' u_i'}}}{\bar{a}} = \frac{u'_{rms}\sqrt{3}}{\bar{a}}, \tag{3.1a}$$

$$Re_\lambda := \frac{\bar{\rho}\,\sqrt{u'_{rms}}\,\lambda_\parallel}{\bar{\mu}}; \quad \lambda_\parallel := \sqrt{\frac{\overline{u'^2}}{\overline{\left(\dfrac{\partial u'}{\partial x}\right)^2}}}. \tag{3.1b,c}$$

These data were made available with a precision of 4 significant digits (D. A. Donzis, 2016, Private communication, lower precision was found inadequate for use in the approximate relations developed in the paper), and cover the range $Re_\lambda \in [35, 430]$ and $M_T \in [0.1, 0.6]$, with a corresponding range of $\mathrm{CV}_{\rho'} \in [0.004, 0.157]$ (Donzis & Jagannathan 2013, table 1, p. 225). The ratios $\mathrm{CV}_{\rho'}^{-1}\mathrm{CV}_{p'}$ and $\mathrm{CV}_{\rho'}^{-1}\mathrm{CV}_{T'}$ vary slightly with M_T and Re_λ (figure 2). This dependency notwithstanding, in this flow, relative variations of temperature are weaker than relative variations of density ($0.35\,\mathrm{CV}_{\rho'} \lessapprox \mathrm{CV}_{T'} \lessapprox 0.4\,\mathrm{CV}_{\rho'}$; figure 2) whereas relative variations of pressure are stronger ($1.3\,\mathrm{CV}_{\rho'} \lessapprox \mathrm{CV}_{p'} \lessapprox 1.4\,\mathrm{CV}_{\rho'}$; figure 2).

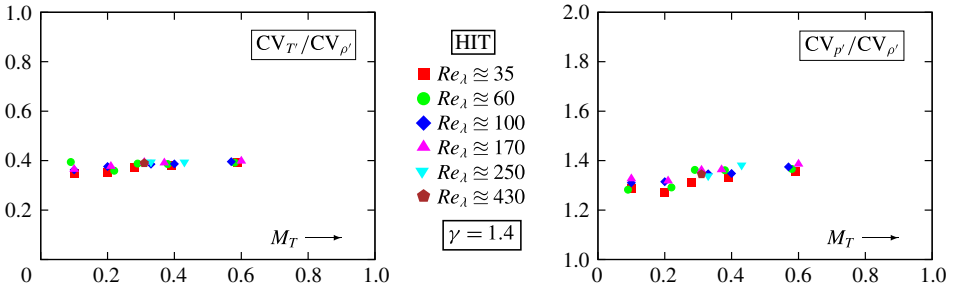

FIGURE 2. (Colour online) Sustained homogeneous isotropic turbulence (HIT) DNS data (Donzis & Jagannathan 2013; D. A. Donzis, 2016, Private communication; Jagannathan & Donzis 2016) for the magnitude of the ratios of the coefficients of variation of temperature $\mathrm{CV}_{T'}$ and pressure $\mathrm{CV}_{p'}$ to the coefficient of variation of density $\mathrm{CV}_{\rho'}$, as a function of the turbulent Mach number $M_T \in [0.1, 0.6]$, for different values of $Re_\lambda \in [35, 430]$.

3.2. *Compressible turbulent plane channel flow*

The DNS data for compressible turbulent plane channel flow were obtained (Gerolymos & Vallet 2014) using a high-order solver (Gerolymos, Sénéchal & Vallet 2010). The flow is modelled by the compressible Navier–Stokes equations (Gerolymos & Vallet 2014, (2.1), p. 706), without bulk viscosity $\mu_b = 0$ (Gerolymos & Vallet 2014, (2.1e), p. 706). The working medium is air, following the equation of state (1.1) with a constant ratio of specific heats (1.1) $\gamma = 1.4$, and Sutherland-like laws for the dynamic viscosity $\mu(T)$ and heat conductivity $\lambda(T)$ (Gerolymos & Vallet 2014, p. 706). The data used in the paper include both data from these computations (Gerolymos & Vallet 2014) and new unpublished data (table 1). The relevant Mach number is the mean centreline Mach number (Gerolymos & Vallet 2014, figure 1, p. 713)

$$\bar{M}_{CL} := \overline{\left(\frac{u_{CL}}{a_{CL}}\right)}, \tag{3.2a}$$

where u is the streamwise velocity, a is the sound speed and $(\cdot)_{CL}$ denotes values at the centreline $y = \delta$. Following Huang *et al.* (1995) we use mixed wall-local scaling (HCB-scaling), based on skin friction $\bar{\tau}_w$ along with the local mean density $\bar{\rho}(y)$ and mean viscosity $\bar{\mu}(y)$, for the non-dimensional wall distance and corresponding Reynolds number

$$y^\star := \frac{\bar{\rho}(y)\sqrt{\dfrac{\bar{\tau}_w}{\bar{\rho}(y)}}(y - y_w)}{\bar{\mu}(y)} = \frac{\sqrt{\bar{\rho}^+(y)}}{\bar{\mu}^+(y)} y^+; \quad Re_{\tau^\star} := \delta^\star = \frac{\sqrt{\bar{\rho}^+_{CL}}}{\bar{\mu}^+_{CL}}\delta^+, \tag{3.2b,c}$$

where $(\cdot)_w$ denotes wall values and

$$y^+ := \frac{\bar{\rho}_w\sqrt{\dfrac{\bar{\tau}_w}{\bar{\rho}_w}}(y - y_w)}{\bar{\mu}_w}; \quad Re_{\tau_w} := \delta^+; \quad \bar{\rho}^+ := \frac{\bar{\rho}}{\bar{\rho}_w}; \quad \bar{\mu}^+ := \frac{\bar{\mu}}{\bar{\mu}_w} \tag{3.2d–g}$$

are the usual incompressible-flow inner-scaled variables (Gerolymos & Vallet 2014, (3.2), p. 714).

Medium box (MB) $L_x \times L_y \times L_z = 8\pi\delta \times 2\delta \times 4\pi\delta$										
$Re_{\tau^\star}$	$\bar{M}_{CL}$	Re_{τ_w}	$N_x \times N_y \times N_z$	Δx^+	Δy_w^+	$N_{y^+\leqslant 10}$	Δy_{CL}^+	Δz^+	$\Delta t^+ = \Delta t_s^+$	t_{OBS}^+
78	1.48	115	$201 \times 121 \times 321$	14.5	0.18	23	3.4	4.5	0.009217	801
106	0.79	117	$257 \times 129 \times 385$	11.5	0.19	22	3.0	3.8	0.013862	2492
113	1.51	169	$257 \times 129 \times 385$	16.6	0.22	21	4.7	5.5	0.015085	1463
98	2.00	219	$401 \times 169 \times 557$	13.8	0.18	24	4.4	4.9	0.010975	1231
112	2.48	493	$801 \times 241 \times 1201$	15.5	0.19	21	5.4	5.2	0.007226	380
177	0.35	180	$257 \times 129 \times 385$	17.6	0.23	20	5.0	5.9	0.006564	869
169	0.79	187	$421 \times 149 \times 801$	11.2	0.19	22	4.1	2.9	0.012942	1058
151	1.50	227	$345 \times 137 \times 529$	16.6	0.23	19	5.6	5.4	0.016696	1010
341	1.52	521	$801 \times 241 \times 1201$	16.4	0.20	21	5.7	5.5	0.014355	894

TABLE 1. Parameters of the DNS computations (L_x, L_y, L_z (N_x, N_y, N_z) are the dimensions (number of grid points) of the computational domain ($x =$ homogeneous streamwise, $y =$ wall-normal, $z =$ homogeneous spanwise direction); δ is the channel half-height; $(\cdot)^+$ denotes wall units; Δx^+, Δy_w^+, Δy_{CL}^+, Δz^+ are the mesh sizes; $(\cdot)_w$ denotes wall and $(\cdot)_{CL}$ centreline values; $N_{y^+\leqslant 10}$ is the number of grid points between the wall and $y^+ = 10$; $\bar{M}_{CL}$ is the centreline Mach number (3.2*a*); $Re_{\tau^\star} := \sqrt{\bar{\rho}_{CL}\,\bar{\tau}_w}\delta\bar{\mu}_{CL}^{-1}$ is the friction Reynolds number in HCB-scaling (3.2*b*,*c*); $Re_{\tau_w} := \sqrt{\bar{\rho}_w\,\bar{\tau}_w}\delta\bar{\mu}_w^{-1}$ is the friction Reynolds number (3.2*d*–*g*); Δt^+ is the computational time step; t_{OBS}^+ is the observation period over which single-point statistics were computed; Δt_s^+ is the sampling time step for the single-point statistics).

The coefficients of variation $\{\mathrm{CV}_{p'}, \mathrm{CV}_{\rho'}, \mathrm{CV}_{T'}\}$ are of the same order of magnitude everywhere in the channel (figure 3), and for all $(Re_{\tau^\star}, \bar{M}_{CL})$ that were investigated, even at the low Mach number limit. Notice that previously published results (Gerolymos & Vallet 2014, figure 6, p. 721) indicate that the correlation coefficients between thermodynamic variables plotted against $y^\star$ (3.2*b*,*c*) show little dependence on $\bar{M}_{CL}$, except perhaps very near the wall ($y^\star < 10$). Nonetheless, in the neighbourhood of the near-wall $\mathrm{CV}_{\rho'}$ peak (Gerolymos & Vallet 2014, $7 \lessapprox y^* \lessapprox 20$, figure 5, p. 720), $\mathrm{CV}_{\rho'} \approxeq 5\mathrm{CV}_{p'}$ (figure 3), so that the assumption $O(\mathrm{CV}_{\rho'}) = O(\mathrm{CV}_{p'})$ (2.2) is stretched to the limit. On the contrary, $O(\mathrm{CV}_{\rho'}) = O(\mathrm{CV}_{T'})$ is satisfied practically everywhere, except very near the wall ($y^\star \lessapprox 1$; figure 3) where the strictly isothermal wall boundary condition enforces $[\mathrm{CV}_{T'}]_w = 0$ at the wall ($y^* = 0$). The question is naturally raised, how a less stringent isothermal-in-the-mean wall boundary condition, where $T_w' \neq 0$ but instead only $\bar{T}_w = \text{const.}$ in the mean is enforced, would modify the viscous sublayer thermodynamic turbulence, and this will be the subject of a future study. Nonetheless, DNS data (Gerolymos & Vallet 2014, figure 5, p. 720) suggest that the boundary condition effect is confined very near the wall ($y^* \lessapprox 1$), and this is further confirmed in § 6.

3.3. *Shear turbulence is not polytropic*

Near the centreline, where the wall influence is weak, channel DNS data (figure 3) indicate that the relative magnitudes of the coefficients of variation $\{\mathrm{CV}_{\rho'}, \mathrm{CV}_{T'}, \mathrm{CV}_{p'}\}$ approach those observed in the HIT DNS data (figure 2), the more so as $Re_{\tau^\star} = \delta^\star$ (3.2*b*,*c*) increases. On the other hand, close to the wall ($y^\star \lessapprox 100$) there are substantial differences. Whereas in HIT (figure 2) and near the centreline in channel flow (figure 3), $\mathrm{CV}_{p'} > \mathrm{CV}_{\rho'} > \mathrm{CV}_{T'}$, near the solid wall $\mathrm{CV}_{\rho'} \approxeq \mathrm{CV}_{T'} > \mathrm{CV}_{p'}$ ($5 \lessapprox y^\star \lessapprox 50$; figure 3). This difference is easily explained by the approximate leading-order relation

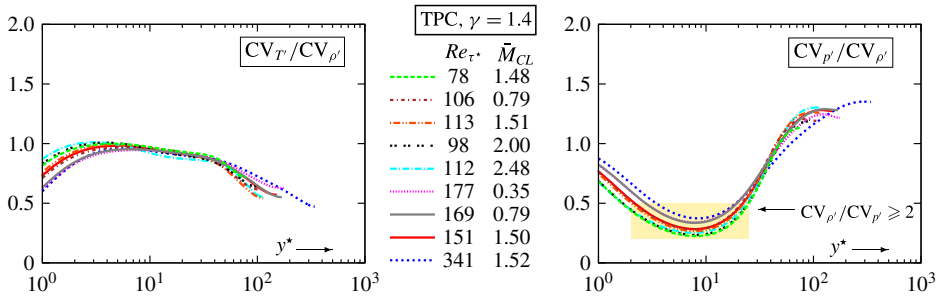

FIGURE 3. (Colour online) Compressible fully developed turbulent plane channel (TPC) flow DNS data (Gerolymos & Vallet 2014) for the magnitude of the ratios of the coefficients of variation of temperature $\mathrm{CV}_{T'}$ and pressure $\mathrm{CV}_{p'}$ to the coefficient of variation of density $\mathrm{CV}_{\rho'}$, as a function of the HCB-scaled wall distance $y^\star$ (3.2*b*,*c*), for different values of $Re_{\tau^\star} \in [78, 341]$ and $\bar{M}_{CL} \in [0.3, 2.5]$ (Gerolymos & Vallet 2014, the shaded region corresponds to values $\mathrm{CV}_{\rho'} \geqslant 2\mathrm{CV}_{p'}$ observed in the neighbourhood of the $\mathrm{CV}_{\rho'}$-peak; figure 5, p. 720).

(Donzis & Jagannathan 2013, (3.4), p. 226) $\mathrm{CV}_{p'}^2 \approxeq \mathrm{CV}_{\rho'}^2 + \mathrm{CV}_{T'}^2 + 2\,c_{\rho'T'}\,\mathrm{CV}_{\rho'}\,\mathrm{CV}_{T'}$ (4.4). In HIT (Donzis & Jagannathan 2013, table 1, p. 225) and in channel flow near the centreline (Gerolymos & Vallet 2014, figure 6, p. 721), the correlation coefficient (2.3*a*) $c_{\rho'T'} > 0 \implies \mathrm{CV}_{p'}^2 > \mathrm{CV}_{\rho'}^2 + \mathrm{CV}_{T'}^2$, whereas near the solid wall (Gerolymos & Vallet 2014, $y^\star \lessapprox 100$, figure 6, p. 721) $c_{\rho'T'} < 0 \implies \mathrm{CV}_{p'}^2 < \mathrm{CV}_{\rho'}^2 + \mathrm{CV}_{T'}^2$.

The difference in behaviour between HIT and near-wall turbulence is further highlighted by considering polytropic exponents, in line with Donzis & Jagannathan (2013, figure 7, p. 234). If turbulence were polytropic ($p \propto \rho^{n_P}$), then, to leading order, specific relations should hold between CVs (Barre & Bonnet 2015, p. 331)

$$p \propto \rho^{n_P} \overset{(1.1)}{\implies} n_P \approxeq \underbrace{\frac{\mathrm{CV}_{p'}}{\mathrm{CV}_{\rho'}}}_{n_{P_{p'\rho'}}} \approxeq \underbrace{1 + \frac{\mathrm{CV}_{T'}}{\mathrm{CV}_{\rho'}}}_{n_{P_{\rho'T'}} > 1}. \tag{3.3}$$

Notice that expression (3.3) which is used in compressible turbulence, both for instantaneous fluctuations (Rubesin 1976) or on the average (Blaisdell *et al.* 1993) is a leading-order approximation of a polytropic process. In practice, $n_{P_{p'\rho'}}$ and $n_{P_{\rho'T'}}$ are never equal (3.3). Gatski & Bonnet (2009, p. 74) suggest considering $n_{P_{p'\rho'}}$ and $n_{P_{\rho'T'}}$ (3.3) as independent parameters, but still $n_{P_{p'\rho'}} \neq n_{P_{\rho'T'}}$ implies that turbulence does not follow a polytropic behaviour.

In HIT both expressions (3.3) are reasonably consistent one with another (figure 4), and although the process is not isentropic the departure from the isentropic value $\gamma = 1.4$ is not very large. On the contrary, wall turbulence is very far from isentropic (figure 4). Furthermore, for $y^\star \lessapprox 100$, the polytropic exponent estimate $n_P(\mathrm{CV}_{\rho'}, \mathrm{CV}_{T'}) \approxeq n_{P_{\rho'T'}} > 1$ is substantially higher than the isentropic value (figure 4), whereas the polytropic exponent estimate $n_P(\mathrm{CV}_{p'}, \mathrm{CV}_{\rho'}) \approxeq n_{P_{p'\rho'}}$ is substantially lower than the isentropic value (figure 4). Therefore, not only is wall turbulence not isentropic, but it cannot be approximated by a polytropic process, which would require the two estimates of n_P (3.3) to be approximately the same. It is not always recognized that the equality $n_{P_{p'\rho'}} \approxeq n_{P_{\rho'T'}}$ can only be achieved under very specific

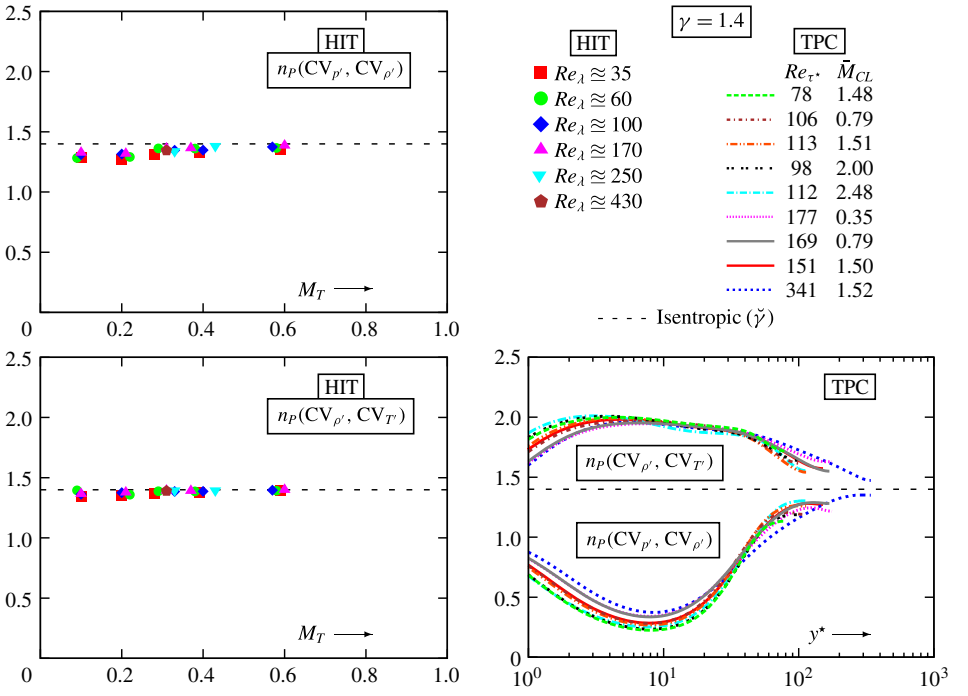

FIGURE 4. (Colour online) Estimates $n_P(\mathrm{CV}_{p'}, \mathrm{CV}_{\rho'}) \approxeq n_{P_{p'\rho'}}$ and $n_P(\mathrm{CV}_{\rho'}, \mathrm{CV}_{T'}) \approxeq n_{P_{\rho'T'}}$ by (3.3) of an eventual representative polytropic exponent, from DNS data of sustained homogeneous isotropic turbulence (HIT) simulations (Donzis & Jagannathan 2013; D. A. Donzis, 2016, Private communication; Jagannathan & Donzis 2016) versus the turbulent Mach number $M_T \in [0.1, 0.6]$ and for compressible fully developed turbulent plane channel (TPC) flow (Gerolymos & Vallet 2014) versus the HCB-scaled wall distance $y^\star$ (3.2*b*,*c*) (for different values of $Re_{\tau^\star} \in [78, 341]$ and $\bar{M}_{CL} \in [0.3, 2.5]$).

conditions. To leading order, straightforward calculation of the difference $n^2_{P_{\rho'T'}} - n^2_{P_{p'\rho'}}$ (3.3), readily yields, using (4.4),

$$(3.3),\,(4.4) \implies n^2_{P_{\rho'T'}} - n^2_{P_{p'\rho'}} \approxeq 2(1 - c_{\rho'T'})\frac{\mathrm{CV}_{T'}}{\mathrm{CV}_{\rho'}} \overset{(2.3b)}{>} 0. \tag{3.4}$$

Therefore, turbulence can only be approximated by a polytropic process iff $c_{\rho'T'} \approxeq +1$, since the alternative condition $\mathrm{CV}_{T'} \ll \mathrm{CV}_{\rho'}$ contradicts conjecture (2.2) and DNS data (figures 2 and 3). Consistent with (3.4), the observed non-polytropic behaviour of thermodynamic fluctuations (figure 4) is explained by the $c_{\rho'T'}$-data. In HIT (Donzis & Jagannathan 2013, table 1, p. 225) $0.6 \lessapprox c_{\rho'T'} \lessapprox 1$ (approaching 1 with increasing M_T): the 2 polytropic exponent estimates are close one to another, and their difference decreases with increasing M_T (figure 4). In channel flow (Gerolymos & Vallet 2014, figure 6, p. 721) $c_{\rho'T'} < 0\,\forall y^\star \lessapprox 100$ (it might approach 1 at high $Re_{\tau^\star}$ at the centreline): the 2 polytropic exponent estimates are largely different, except when approaching the centreline for the higher $Re_{\tau^\star}$ (figure 4). This discussion highlights the importance of the correlation coefficient $c_{\rho'T'}$ on thermodynamic turbulence structure, and is further investigated in § 6.

4. Leading-order approximations of correlation coefficients

To obtain estimates of approximation errors, we built approximations by asymptotically expanding the exact relations (2.5), (2.9).

4.1. *Approximation of correlation coefficients* $\{c_{p'\rho'}, c_{p'T'}, c_{\rho'T'}\}$

Using again the order-of-magnitude relation (2.2), the system (2.5) is readily expanded as

$$\mathrm{CV}_{p'} - c_{p'\rho'}\,\mathrm{CV}_{\rho'} - c_{p'T'}\,\mathrm{CV}_{T'} \overset{(2.5a)}{\sim} c_{p'\rho'T'}\,\mathrm{CV}_{\rho'}\,\mathrm{CV}_{T'} + O(\mathrm{CV}_{\rho'}\mathrm{CV}_{T'}\mathrm{CV}_{p'}), \tag{4.1a}$$

$$c_{p'\rho'}\,\mathrm{CV}_{p'} - \mathrm{CV}_{\rho'} - c_{\rho'T'}\,\mathrm{CV}_{T'} \overset{(2.5b)}{\sim} c_{\rho'\rho'T'}\,\mathrm{CV}_{\rho'}\,\mathrm{CV}_{T'} + O(\mathrm{CV}_{\rho'}\mathrm{CV}_{T'}\mathrm{CV}_{p'}), \tag{4.1b}$$

$$c_{p'T'}\,\mathrm{CV}_{p'} - c_{\rho'T'}\,\mathrm{CV}_{\rho'} - \mathrm{CV}_{T'} \overset{(2.5c)}{\sim} c_{\rho'T'T'}\,\mathrm{CV}_{\rho'}\,\mathrm{CV}_{T'} + O(\mathrm{CV}_{\rho'}\mathrm{CV}_{T'}\mathrm{CV}_{p'}), \tag{4.1c}$$

where the right-hand side terms represent the leading error of the approximation with the higher-order terms being by (2.2) $O(\mathrm{CV}_{\rho'}\mathrm{CV}_{T'}\mathrm{CV}_{p'}) = O(\mathrm{CV}^3_{\rho'})$. The linear system (4.1) for the 2-moment correlation coefficients, can be readily solved to obtain

$$c_{p'\rho'} \overset{(4.1),\,(\mathrm{A}\,1a)}{\sim} +\frac{1}{2}\frac{\mathrm{CV}_{p'}}{\mathrm{CV}_{\rho'}} + \frac{1}{2}\frac{\mathrm{CV}_{\rho'}}{\mathrm{CV}_{p'}} - \frac{1}{2}\frac{\mathrm{CV}_{T'}}{\mathrm{CV}_{p'}}\frac{\mathrm{CV}_{T'}}{\mathrm{CV}_{\rho'}} - c_{\rho'T'T'}\frac{\mathrm{CV}^2_{T'}}{\mathrm{CV}_{p'}} + O\left(\mathrm{CV}^2_{\rho'}\right), \tag{4.2a}$$

$$c_{p'T'} \overset{(4.1),\,(\mathrm{A}\,1a)}{\sim} +\frac{1}{2}\frac{\mathrm{CV}_{T'}}{\mathrm{CV}_{p'}} + \frac{1}{2}\frac{\mathrm{CV}_{p'}}{\mathrm{CV}_{T'}} - \frac{1}{2}\frac{\mathrm{CV}_{\rho'}}{\mathrm{CV}_{p'}}\frac{\mathrm{CV}_{\rho'}}{\mathrm{CV}_{T'}} - c_{\rho'\rho'T'}\frac{\mathrm{CV}^2_{\rho'}}{\mathrm{CV}_{p'}} + O\left(\mathrm{CV}^2_{\rho'}\right), \tag{4.2b}$$

$$c_{\rho'T'} \overset{(4.1),\,(\mathrm{A}\,1a)}{\sim} -\frac{1}{2}\frac{\mathrm{CV}_{\rho'}}{\mathrm{CV}_{T'}} - \frac{1}{2}\frac{\mathrm{CV}_{T'}}{\mathrm{CV}_{\rho'}} + \frac{1}{2}\frac{\mathrm{CV}_{p'}}{\mathrm{CV}_{\rho'}}\frac{\mathrm{CV}_{p'}}{\mathrm{CV}_{T'}} - c_{p'\rho'T'}\,\mathrm{CV}_{p'} + O\left(\mathrm{CV}^2_{\rho'}\right), \tag{4.2c}$$

where (A 1*a*) was used to simplify the expression of the leading terms of the approximation error. The nonlinear higher-order terms are formally identified as $O(\mathrm{CV}^3_{\rho'})$ in (4.1) and $O\left(\mathrm{CV}^2_{\rho'}\right)$ in (4.2), using (2.2).

Retaining only $O(1)$ terms in (4.2) yields the approximations

$$c_{p'\rho'} \overset{(4.2a)}{\approx} +\frac{1}{2}\frac{\mathrm{CV}_{p'}}{\mathrm{CV}_{\rho'}} + \frac{1}{2}\frac{\mathrm{CV}_{\rho'}}{\mathrm{CV}_{p'}} - \frac{1}{2}\frac{\mathrm{CV}_{T'}}{\mathrm{CV}_{p'}}\frac{\mathrm{CV}_{T'}}{\mathrm{CV}_{\rho'}} + O\left(\frac{\mathrm{CV}^2_{T'}}{\mathrm{CV}_{p'}}\right), \tag{4.3a}$$

$$c_{p'T'} \overset{(4.2b)}{\approx} +\frac{1}{2}\frac{\mathrm{CV}_{T'}}{\mathrm{CV}_{p'}} + \frac{1}{2}\frac{\mathrm{CV}_{p'}}{\mathrm{CV}_{T'}} - \frac{1}{2}\frac{\mathrm{CV}_{\rho'}}{\mathrm{CV}_{p'}}\frac{\mathrm{CV}_{\rho'}}{\mathrm{CV}_{T'}} + O\left(\frac{\mathrm{CV}^2_{\rho'}}{\mathrm{CV}_{p'}}\right), \tag{4.3b}$$

$$c_{\rho'T'} \overset{(4.2c)}{\approx} -\frac{1}{2}\frac{\mathrm{CV}_{\rho'}}{\mathrm{CV}_{T'}} - \frac{1}{2}\frac{\mathrm{CV}_{T'}}{\mathrm{CV}_{\rho'}} + \frac{1}{2}\frac{\mathrm{CV}_{p'}}{\mathrm{CV}_{\rho'}}\frac{\mathrm{CV}_{p'}}{\mathrm{CV}_{T'}} + O\left(\mathrm{CV}_{p'}\right). \tag{4.3c}$$

Notice that (4.3*c*) is equivalent to the approximate leading-order relation (Donzis & Jagannathan 2013, (3.4), p. 226)

$$\mathrm{CV}^2_{p'} \approx \mathrm{CV}^2_{\rho'} + \mathrm{CV}^2_{T'} + 2\,c_{\rho'T'}\,\mathrm{CV}_{\rho'}\,\mathrm{CV}_{T'} + O(\mathrm{CV}_{p'}\,\mathrm{CV}_{\rho'}\,\mathrm{CV}_{T'}). \tag{4.4}$$

4.2. *Approximation of entropy variance and correlations*

Expansion (2.9) can be readily truncated to yield the approximations

$$\frac{s'_{rms}}{R_g} \overset{(2.9),\,(2.2)}{\approx} \sqrt{\frac{\breve{\gamma}}{(\breve{\gamma}-1)^2}\,\mathrm{CV}_{T'}^2 + \frac{\breve{\gamma}}{\breve{\gamma}-1}\,\mathrm{CV}_{\rho'}^2 - \frac{1}{\breve{\gamma}-1}\,\mathrm{CV}_{p'}^2} + O\left(\mathrm{CV}_{T'}^2,\, \frac{\max\left(\mathrm{CV}_{\rho'}^3, \mathrm{CV}_{T'}^3, \mathrm{CV}_{p'}^3\right)}{R_g^{-1}\, s'_{rms}}\right) \tag{4.5a}$$

$$\overset{(4.4),\,(2.2)}{\approx} \sqrt{\frac{1}{(\breve{\gamma}-1)^2}\,\mathrm{CV}_{T'}^2 + \mathrm{CV}_{\rho'}^2 - \frac{2}{\breve{\gamma}-1}\,c_{\rho'T'}\,\mathrm{CV}_{\rho'}\,\mathrm{CV}_{T'}} + O\left(\mathrm{CV}_{T'}^2,\, \frac{\max\left(\mathrm{CV}_{\rho'}^3, \mathrm{CV}_{T'}^3, \mathrm{CV}_{\rho'}\,\mathrm{CV}_{T'}\,\mathrm{CV}_{p'}\right)}{R_g^{-1}\, s'_{rms}}\right). \tag{4.5b}$$

The expression inside the radical in (4.5*b*) is always $\geqslant 0$ because $\left|c_{\rho'T'}\right| \leqslant 1$ (2.3*a*). The leading terms $O(\mathrm{CV}_{\rho'}^3,\ \mathrm{CV}_{T'}^3,\ \mathrm{CV}_{p'}^3,\ \mathrm{CV}_{T'}^2\, R_g^{-1}\, s'_{rms})$ of the approximation error of $R_g^{-2}\, s'^2_{rms}$ (2.9), do not contain ratios but only positive powers of coefficients of variation, in the same way as the $c_{\rho'T'}$ approximation (4.2*c*), and therefore (2.9), is expected to be quite reliable. This remark obviously applies to the approximation (4.5), where the appearance of s'_{rms} at the denominator of the error is formal, by the expansion of $\sqrt{\cdot}$ of (2.9).

Multiplying (2.8*b*) by ρ' or T' yields, upon averaging, using definitions (2.1), (2.3) and truncating to leading order

$$c_{s'\rho'}\frac{s'_{rms}}{R_g} \overset{(2.8b)}{\sim} \frac{1}{\breve{\gamma}-1}\,c_{\rho'T'}\,\mathrm{CV}_{T'} - \mathrm{CV}_{\rho'} + O\left(\mathrm{CV}_{\rho'}^2, \mathrm{CV}_{T'}^2\right), \tag{4.6a}$$

$$c_{s'T'}\frac{s'_{rms}}{R_g} \overset{(2.8b)}{\sim} \frac{1}{\breve{\gamma}-1}\,\mathrm{CV}_{T'} - c_{\rho'T'}\,\mathrm{CV}_{\rho'} + O\left(\mathrm{CV}_{\rho'}^2, \mathrm{CV}_{T'}^2\right). \tag{4.6b}$$

Multiplying (2.4) by s' yields, upon averaging, using definitions (2.1), (2.3) and truncating to leading order

$$c_{s'p'}\,\mathrm{CV}_{p'} \overset{(2.4)}{\sim} c_{s'\rho'}\,\mathrm{CV}_{\rho'} + c_{s'T'}\,\mathrm{CV}_{T'} + O\left(\mathrm{CV}_{\rho'}\,\mathrm{CV}_{T'}\right) \tag{4.6c}$$

$$\overset{(4.6a),\,(4.6b)}{\sim} \frac{1}{R_g^{-1}\, s'_{rms}}\left(-\mathrm{CV}_{\rho'}^2 + \frac{2-\breve{\gamma}}{\breve{\gamma}-1}\,c_{\rho'T'}\,\mathrm{CV}_{\rho'}\,\mathrm{CV}_{T'} + \frac{1}{\breve{\gamma}-1}\,\mathrm{CV}_{T'}^2\right) + O\left(\mathrm{CV}_{\rho'}\,\mathrm{CV}_{T'}, \frac{\max\left(\mathrm{CV}_{\rho'}^3, \mathrm{CV}_{T'}^3\right)}{R_g^{-1}\, s'_{rms}}\right). \tag{4.6d}$$

Using the leading-order approximations (4.3*c*) for $c_{\rho'T'}$ and (4.5*b*) in (4.6) yields the leading-order approximations

$$c_{s'\rho'} \overset{(4.6a),\,(4.5),\,(4.2c)}{\approx} \frac{1}{2}\frac{-\frac{2\breve{\gamma}-1}{\breve{\gamma}-1}\mathrm{CV}^2_{\rho'}-\frac{1}{\breve{\gamma}-1}\mathrm{CV}^2_{T'}+\frac{1}{\breve{\gamma}-1}\mathrm{CV}^2_{p'}}{\mathrm{CV}_{\rho'}\sqrt{\frac{\breve{\gamma}}{(\breve{\gamma}-1)^2}\mathrm{CV}^2_{T'}+\frac{\breve{\gamma}}{\breve{\gamma}-1}\mathrm{CV}^2_{\rho'}-\frac{1}{\breve{\gamma}-1}\mathrm{CV}^2_{p'}}} + O\left(\frac{\max\left(\mathrm{CV}^2_{\rho'},\mathrm{CV}^2_{T'},\mathrm{CV}_{T'}\mathrm{CV}_{p'}\right)}{R_g^{-1}\,s'_{rms}}\right), \tag{4.7a}$$

$$c_{s'T'} \overset{(4.6b),\,(4.5),\,(4.2c)}{\approx} \frac{1}{2}\frac{\mathrm{CV}^2_{\rho'}+\frac{\breve{\gamma}+1}{\breve{\gamma}-1}\mathrm{CV}^2_{T'}-\mathrm{CV}^2_{p'}}{\mathrm{CV}_{T'}\sqrt{\frac{\breve{\gamma}}{(\breve{\gamma}-1)^2}\mathrm{CV}^2_{T'}+\frac{\breve{\gamma}}{\breve{\gamma}-1}\mathrm{CV}^2_{\rho'}-\frac{1}{\breve{\gamma}-1}\mathrm{CV}^2_{p'}}} + O\left(\frac{\max\left(\mathrm{CV}^2_{\rho'},\mathrm{CV}^2_{T'},\mathrm{CV}_{\rho'}\mathrm{CV}_{p'}\right)}{R_g^{-1}\,s'_{rms}}\right), \tag{4.7b}$$

$$c_{s'p'} \overset{(4.6c),\,(4.7a),\,(4.7b)}{\approx} \frac{1}{2}\frac{-\frac{\breve{\gamma}}{\breve{\gamma}-1}\mathrm{CV}^2_{\rho'}+\frac{\breve{\gamma}}{\breve{\gamma}-1}\mathrm{CV}^2_{T'}+\frac{2-\breve{\gamma}}{\breve{\gamma}-1}\mathrm{CV}^2_{p'}}{\mathrm{CV}_{p'}\sqrt{\frac{\breve{\gamma}}{(\breve{\gamma}-1)^2}\mathrm{CV}^2_{T'}+\frac{\breve{\gamma}}{\breve{\gamma}-1}\mathrm{CV}^2_{\rho'}-\frac{1}{\breve{\gamma}-1}\mathrm{CV}^2_{p'}}} + O\left(\frac{\mathrm{CV}_{\rho'}\mathrm{CV}_{T'}}{\mathrm{CV}_{p'}},\frac{\max\left(\mathrm{CV}^3_{\rho'},\mathrm{CV}^3_{T'}\right)}{\mathrm{CV}_{p'}\,R_g^{-1}\,s'_{rms}}\right) \tag{4.7c}$$

for $\{c_{s'\rho'}, c_{s'T'}, c_{s'p'}\}$ in terms of the coefficients of variation $\{\mathrm{CV}_{\rho'}, \mathrm{CV}_{T'}, \mathrm{CV}_{p'}\}$, which of course include $\breve{\gamma}$.

5. Assessment of leading-order approximations against DNS data

DNS data determine the range of validity and robustness of the approximations (4.3), (4.5*a*), (4.7).

5.1. *Approximation accuracy in compressible turbulent plane channel flow*

The leading-order approximations (4.3) are assessed by comparison with DNS data (Gerolymos & Vallet 2014) for channel flow (figures 5–7), but also by comparison with the higher-order expansions (4.2), to analyse the eventual importance of the leading error terms and when necessary to identify the origin of the nonlinearities.

Regarding $c_{\rho'T'}$ (figure 5), the leading-order approximation (4.3*c*) is in excellent agreement with DNS data $\forall\, y^\star$ and for the entire available range of $(Re_{\tau^\star}, \bar{M}_{CL})$. The higher $O(\mathrm{CV}^2_{\rho'})$ expansion of $c_{\rho'T'}$ (4.2*c*) is practically identical to the leading $O(\mathrm{CV}_{\rho'})$ approximation (4.3*c*) and to the DNS data (figure 5), implying that the leading error $-c_{p'\rho'T'}\mathrm{CV}_{p'}$ is indeed negligible, even for the highest $\bar{M}_{CL}\approxeq 2.5$.

Regarding the correlation coefficients involving p', $c_{p'\rho'}$ (figure 6) and $c_{p'T'}$ (figure 7), the leading $O(\mathrm{CV}_{\rho'})$ approximations (4.3*a*), (4.3*b*) are excellent for the subsonic $\bar{M}_{CL}\approxeq 0.8$ case, and remain quite satisfactory at $\bar{M}_{CL}\approxeq 1.5$, the more so with increasing $Re_{\tau^\star}$ (figures 6, 7). For the higher $\bar{M}_{CL}\in\{2, 2.5\}$ cases, the leading $O(\mathrm{CV}_{\rho'})$ approximations (4.3*a*), (4.3*b*) are satisfactory near the wall and in the outer part of the flow, but discrepancies with DNS data appear in the region $10\lessapprox y^\star\lessapprox 40$ (figures 6, 7).

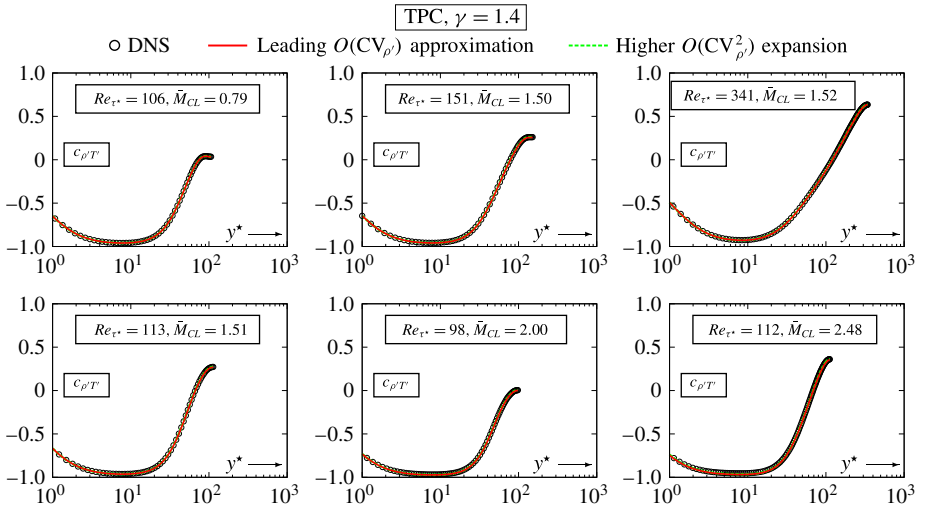

FIGURE 5. (Colour online) Comparison of the leading $O(\mathrm{CV}_{\rho'})$ approximation (4.3*c*) of $c_{\rho'T'}(\mathrm{CV}_{\rho'}, \mathrm{CV}_{T'}, \mathrm{CV}_{p'})$ with DNS data for compressible fully developed turbulent plane channel (TPC) flow (Gerolymos & Vallet 2014), plotted against the HCB-scaled wall distance $y^\star$ (3.2*b*,*c*), for different values of $Re_{\tau^\star} \in [98, 341]$ and $\bar{M}_{CL} \in [0.8, 2.5]$, and with the higher $O(\mathrm{CV}^2_{\rho'})$ expansion (4.2*c*) which uses DNS data for $c_{p'\rho'T'}$.

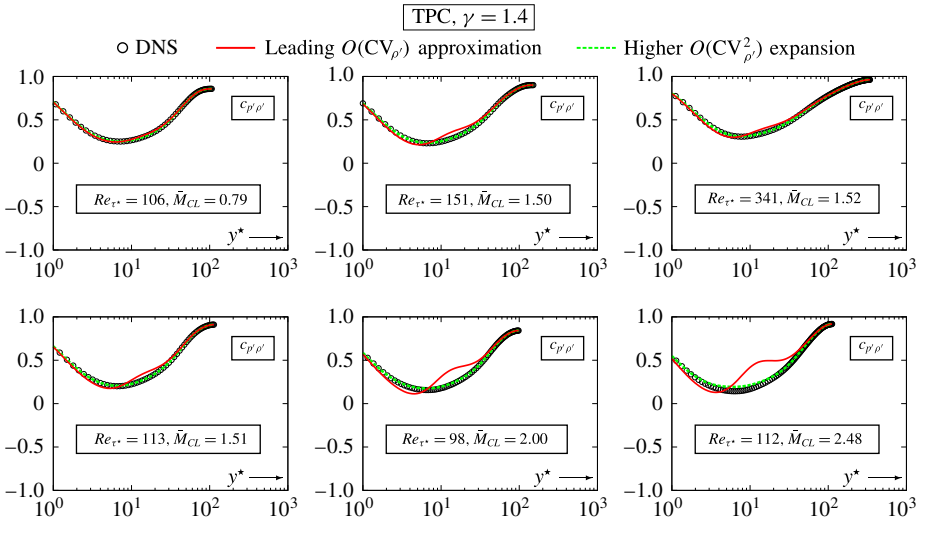

FIGURE 6. (Colour online) Comparison of the leading $O(\mathrm{CV}_{\rho'})$ approximation (4.3*a*) of $c_{p'\rho'}(\mathrm{CV}_{\rho'}, \mathrm{CV}_{T'}, \mathrm{CV}_{p'})$ with DNS data for compressible fully developed turbulent plane channel (TPC) flow (Gerolymos & Vallet 2014), plotted against the HCB-scaled wall distance $y^\star$ (3.2*b*,*c*), for different values of $Re_{\tau^\star} \in [98, 341]$ and $\bar{M}_{CL} \in [0.8, 2.5]$, and with the higher $O(\mathrm{CV}^2_{\rho'})$ expansion (4.2*a*) which uses DNS data for $c_{\rho'T'T'}$.

Both the magnitude of the error and the $y^\star$-range where discrepancies are observed increase with increasing $\bar{M}_{CL} \gtrapprox 2$. These discrepancies are fully accounted for by the leading error of the approximations (4.3*a*), (4.3*b*), because the corresponding by (2.2) $O(\mathrm{CV}^2_{\rho'})$ expansions (4.2*a*), (4.2*b*), which use DNS data for the 3CCs $c_{\rho'T'T'}$

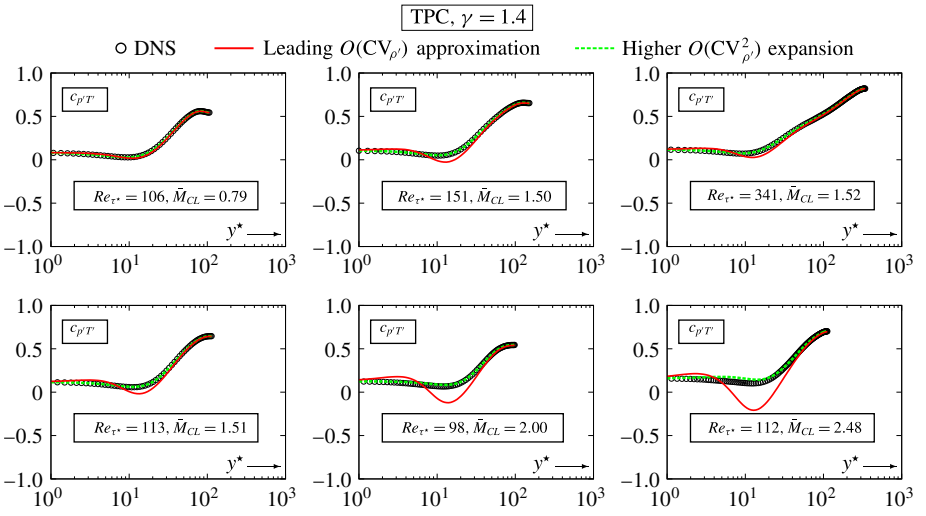

FIGURE 7. (Colour online) Comparison of the leading $O(\mathrm{CV}_{\rho'})$ approximation (4.3*b*) of $c_{p'T'}(\mathrm{CV}_{\rho'}, \mathrm{CV}_{T'}, \mathrm{CV}_{p'})$ with DNS data for compressible fully developed turbulent plane channel (TPC) flow (Gerolymos & Vallet 2014), plotted against the HCB-scaled wall distance $y^\star$ (3.2*b*,*c*), for different values of $Re_{\tau^\star} \in [98, 341]$ and $\bar{M}_{CL} \in [0.8, 2.5]$, and with the higher $O(\mathrm{CV}^2_{\rho'})$ expansion (4.2*b*) which uses DNS data for $c_{\rho'\rho'T'}$.

and $c_{\rho'\rho'T'}$, are in excellent agreement with DNS data (figures 6, 7) $\forall\, y^\star$ and for the entire $(Re_{\tau^\star}, \bar{M}_{CL})$-range studied, a very slight discrepancy observed at $\bar{M}_{CL} \approxeq 2.5$ notwithstanding. The leading error in the approximations (4.3*a*) for $c_{p'\rho'}$ and (4.3*b*) for $c_{p'T'}$ is more important than that for the approximation (4.2*c*) for $c_{\rho'T'}$ because of the presence of the ratios $\mathrm{CV}_{p'}^{-1}\mathrm{CV}_{T'}$ and $\mathrm{CV}_{p'}^{-1}\mathrm{CV}_{\rho'}$ which become $\geqslant 2$ around $5 \leqslant y^\star \leqslant 25$ (figure 3), whereas the leading error in (4.2*c*) for $c_{\rho'T'}$ does not contain ratios between relative amplitudes.

The approximations (4.5*a*), (4.7) are assessed (figures 8–11) against DNS data for compressible channel flow (Gerolymos & Vallet 2014). These data were obtained by computing the instantaneous entropy field $s(\boldsymbol{x}, t)$ exactly (Gerolymos & Vallet 2014, (2.5), p. 710) and sampling (Gerolymos *et al.* 2010, § 4.4, p. 791) the appropriate moments: they involve no approximation or truncation.

The leading-order approximations (4.5*a*) of $R_g^{-1} s'_{rms}$ (figure 8), (4.7*a*) of $c_{s'\rho'}$ (figure 9), and (4.7*b*) of $c_{s'T'}$ (figure 10) are in excellent agreement with DNS data $\forall\, y^\star$ and for every available $(Re_{\tau^\star}, \bar{M}_{CL})$. On the contrary the leading-order approximation (4.7*c*) of $c_{s'p'}$ (figure 11) behaves in a manner similar to the leading-order approximations (4.3*a*), (4.3*b*) of $c_{p'\rho'}$ (figure 6) and of $c_{p'T'}$ (figure 7). It is excellent for $\bar{M}_{CL} \approxeq 0.8$ and satisfactory for $\bar{M}_{CL} \approxeq 1.5$, but presents discrepancies for the higher $\bar{M}_{CL} \in \{2, 2.5\}$ (figure 11), in the range $10 \lessapprox y^\star \lessapprox 40$. Again, the leading error in (4.7*c*) involves division by $\mathrm{CV}_{p'}$ and suffers from the high values of $\mathrm{CV}_{p'}^{-1}\mathrm{CV}_{\rho'}$ and $\mathrm{CV}_{p'}^{-1}\mathrm{CV}_{T'}$ (figure 3).

As a conclusion, nonlinear effects of compressibility seem to influence some features of the thermodynamic correlations containing p' when $\bar{M}_{CL} \gtrapprox 2$ (figures 5–7): in this range, the quadratic terms in the exact relations (2.5) cannot be neglected. Nonetheless, the region where these nonlinear compressibility effects are important remains confined in the buffer zone of the wall layer (Smits & Dussauge 2006, p. 203).

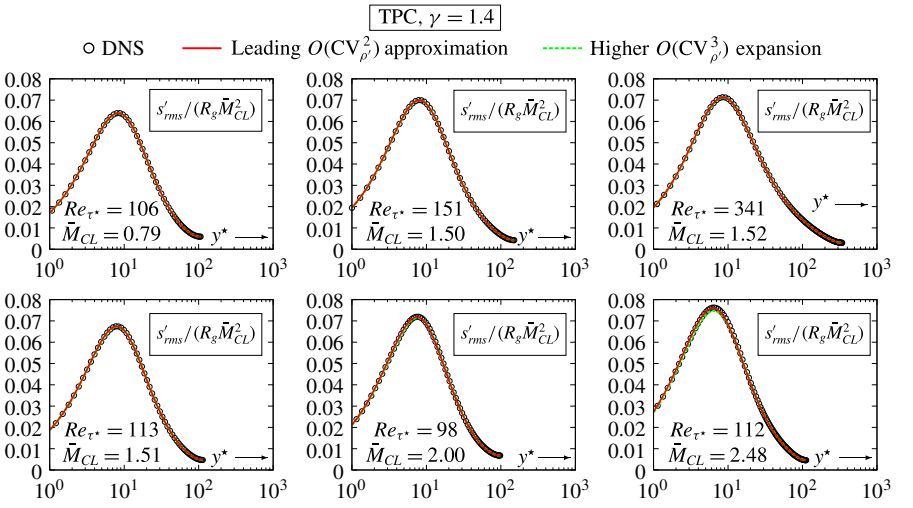

FIGURE 8. (Colour online) Comparison of the leading $O(\mathrm{CV}_{\rho'^2})$ approximation (4.5*a*) of $s'_{rms}(\mathrm{CV}_{\rho'}, \mathrm{CV}_{T'}, \mathrm{CV}_{p'})$ with DNS data for compressible fully developed turbulent plane channel (TPC) flow (Gerolymos & Vallet 2014), plotted against the HCB-scaled wall distance $y^\star$ (3.2*b*,*c*), for different values of $Re_{\tau^\star} \in [98, 341]$ and $\tilde{M}_{CL} \in [0.8, 2.5]$, and with the higher $O(\mathrm{CV}_{\rho'}^3)$ expansion (2.9) which uses DNS data for the skewnesses $\{S_{p'}, S_{\rho'}, S_{T'}\}$.

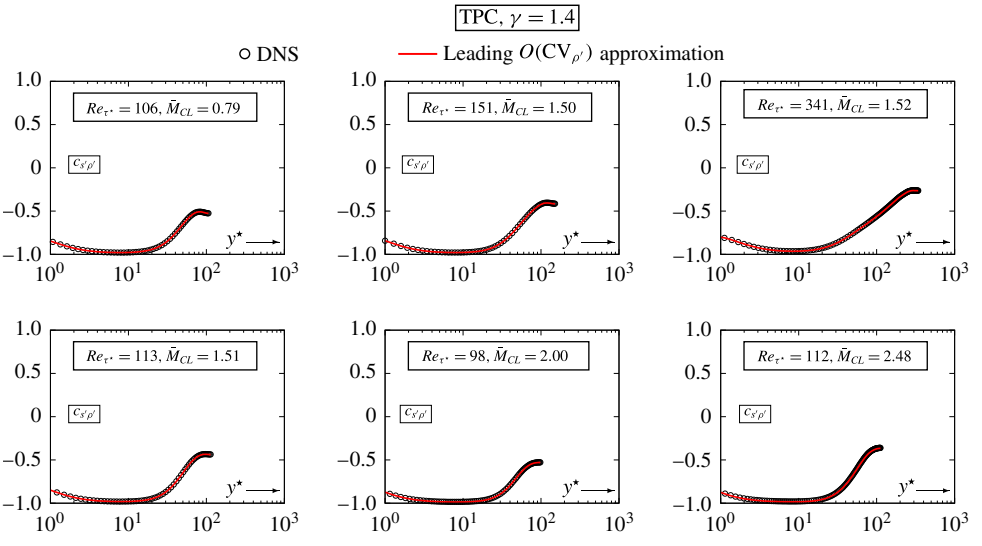

FIGURE 9. (Colour online) Comparison of the leading $O(\mathrm{CV}_{\rho'})$ approximation (4.7*a*) of $c_{s'\rho'}(\mathrm{CV}_{\rho'}, \mathrm{CV}_{T'}, \mathrm{CV}_{p'})$ with DNS data for compressible fully developed turbulent plane channel (TPC) flow (Gerolymos & Vallet 2014), plotted against the HCB-scaled wall distance $y^\star$ (3.2*b*,*c*), for different values of $Re_{\tau^\star} \in [98, 341]$ and $\tilde{M}_{CL} \in [0.8, 2.5]$.

5.2. *Approximation accuracy in sustained compressible HIT*

Only $c_{\rho'T'}$ was available in the HIT DNS database (Donzis & Jagannathan 2013; D. A. Donzis, 2016, Private communication; Jagannathan & Donzis 2016). The

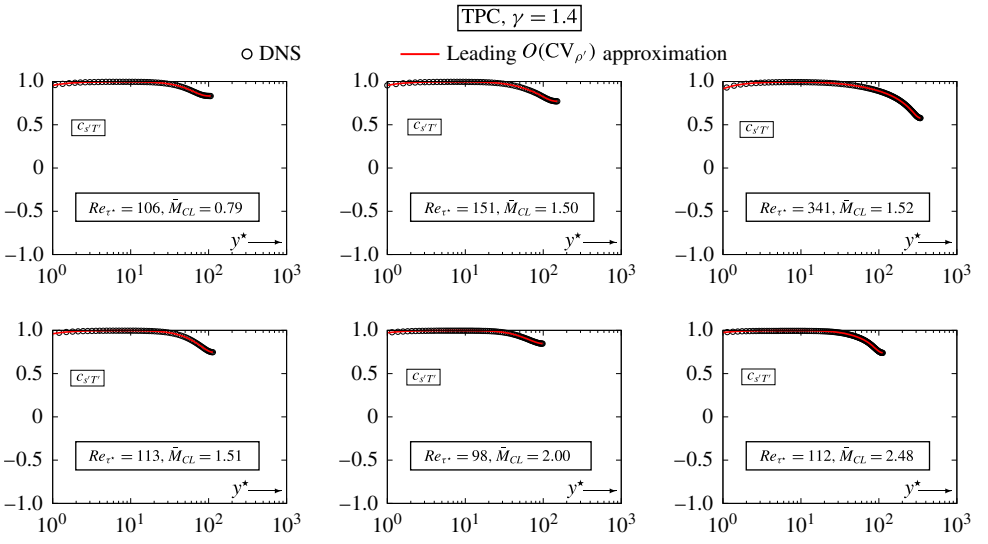

FIGURE 10. (Colour online) Comparison of the leading $O(\mathrm{CV}_{\rho'})$ approximation (4.7*b*) of $c_{s'T'}(\mathrm{CV}_{\rho'}, \mathrm{CV}_{T'}, \mathrm{CV}_{p'})$ with DNS data for compressible fully developed turbulent plane channel (TPC) flow (Gerolymos & Vallet 2014), plotted against the HCB-scaled wall distance $y^\star$ (3.2*b*,*c*), for different values of $Re_{\tau^\star} \in [98, 341]$ and $\bar{M}_{CL} \in [0.8, 2.5]$.

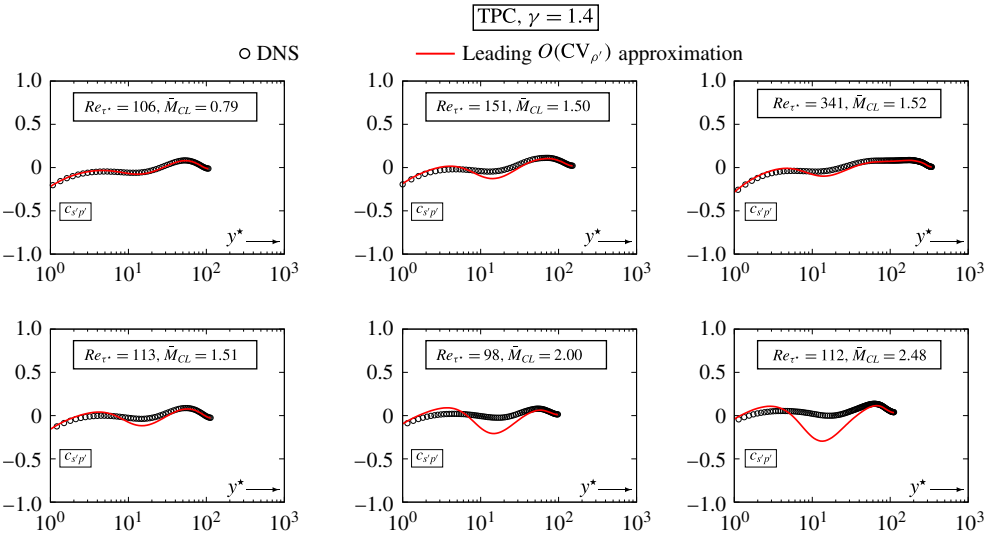

FIGURE 11. (Colour online) Comparison of the leading $O(\mathrm{CV}_{\rho'})$ approximation (4.7*c*) of $c_{s'p'}(\mathrm{CV}_{\rho'}, \mathrm{CV}_{T'}, \mathrm{CV}_{p'})$ with DNS data for compressible fully developed turbulent plane channel (TPC) flow (Gerolymos & Vallet 2014), plotted against the HCB-scaled wall distance $y^\star$ (3.2*b*,*c*), for different values of $Re_{\tau^\star} \in [98, 341]$ and $\bar{M}_{CL} \in [0.8, 2.5]$.

leading-order approximation (4.3*c*) compares very well with the DNS data (figure 12), corroborating the conclusion (§ 5.1) that (4.3*c*) is a very robust approximation. Notice also that the ratios $\mathrm{CV}_{p'}^{-1}\mathrm{CV}_{T'}$ and $\mathrm{CV}_{p'}^{-1}\mathrm{CV}_{\rho'}$ which multiply the leading error of the approximations (4.3*a*) for $c_{p'\rho'}$ and (4.3*b*) for $c_{p'T'}$ are invariably <1 in HIT (figure 2).

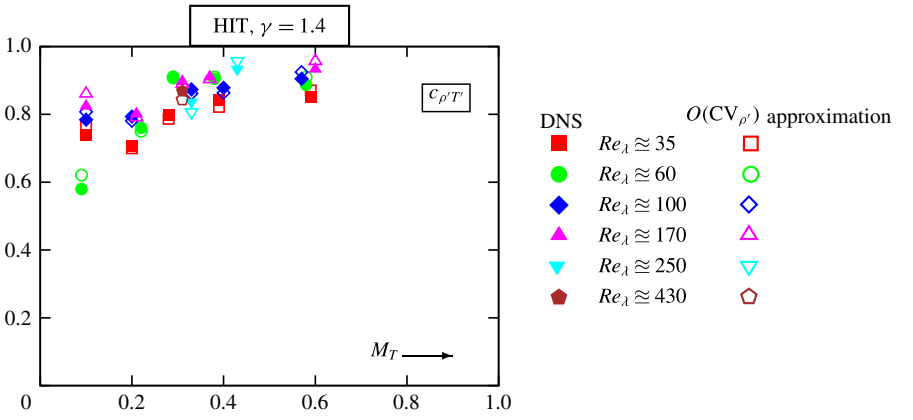

FIGURE 12. (Colour online) Comparison of the leading $O(\mathrm{CV}_{\rho'})$ approximation (4.3*c*) of $c_{\rho'T'}(\mathrm{CV}_{\rho'}, \mathrm{CV}_{T'}, \mathrm{CV}_{p'})$ with sustained homogeneous isotropic turbulence (HIT) DNS data (Donzis & Jagannathan 2013; D. A. Donzis, 2016, Private communication; Jagannathan & Donzis 2016), plotted against the turbulent Mach number $M_T \in [0.1, 0.6]$, for different values of $Re_\lambda \in [35, 430]$ (solid symbols: DNS, open symbols: approximation).

Therefore, we expect that the approximations (4.3*a*), (4.3*b*) of $c_{p'\rho'}$ and $c_{p'T'}$ should be quite accurate for the HIT case. Of course data for these correlations are needed to fully substantiate this conjecture.

The leading-order approximations (4.3), (4.5*a*), (4.7) can be used to discuss the behaviour of compressible HIT, in terms of correlations that were not available in the database (Donzis & Jagannathan 2013; D. A. Donzis, 2016, Private communication; Jagannathan & Donzis 2016). At the highest $M_T \approxeq 0.6$ sustained compressible HIT data (Donzis & Jagannathan 2013, table 1, p. 225), $\mathrm{CV}_{\rho'} \approxeq 0.16$, $\mathrm{CV}_{p'} \approxeq 0.22$ and $\mathrm{CV}_{T'} \approxeq 0.06$. Based on the assessment of the leading-order approximations (4.3), (4.5*a*), (4.7) for compressible channel flow (figures 5–11) we expect these approximations to be reasonably accurate, and use them to investigate the behaviour of compressible HIT with increasing M_T (figure 13). The non-dimensional ratio of entropy and density fluctuations $R_g^{-1}\mathrm{CV}_{\rho'}^{-1}s'_{rms}$ decreases with increasing M_T and shows significant Re_λ-dependency (figure 13), which is not surprising since s'_{rms} is largely the result of dissipative phenomena. The various correlation coefficients depend mainly on M_T, with a weaker Re_λ-dependency (figure 13). We observe in particular that $c_{s'T'} \approxeq 0.2\,\forall\,(M_T, Re_\lambda)$ remains practically constant with little scatter (figure 13). This observation is further confirmed in § 6 and will be used in § 7.1 to suggest a simple model for the thermodynamic turbulence structure of subsonic sustained compressible HIT.

6. Compressible aerodynamic turbulence map

The different approximate expressions developed above (4.3), (4.4), (4.5), (4.7) can be used to map the behaviour of compressible turbulence. We will assume in the following the validity of these leading-order approximations. The important and robust relation (4.4) suggests working in the $(\mathrm{CV}_{\rho'}^{-1}\mathrm{CV}_{T'}, c_{\rho'T'})$-plane (figure 14), limited by (2.3*a*) to $-1 \leqslant c_{\rho'T'} \leqslant +1$.

The abscissa $\mathrm{CV}_{\rho'}^{-1}\mathrm{CV}_{T'}$ separates (figure 14) the region $\mathrm{CV}_{\rho'} > \mathrm{CV}_{T'}$ from the region $\mathrm{CV}_{\rho'} < \mathrm{CV}_{T'}$. Most of the DNS data considered in the paper (§ 3)

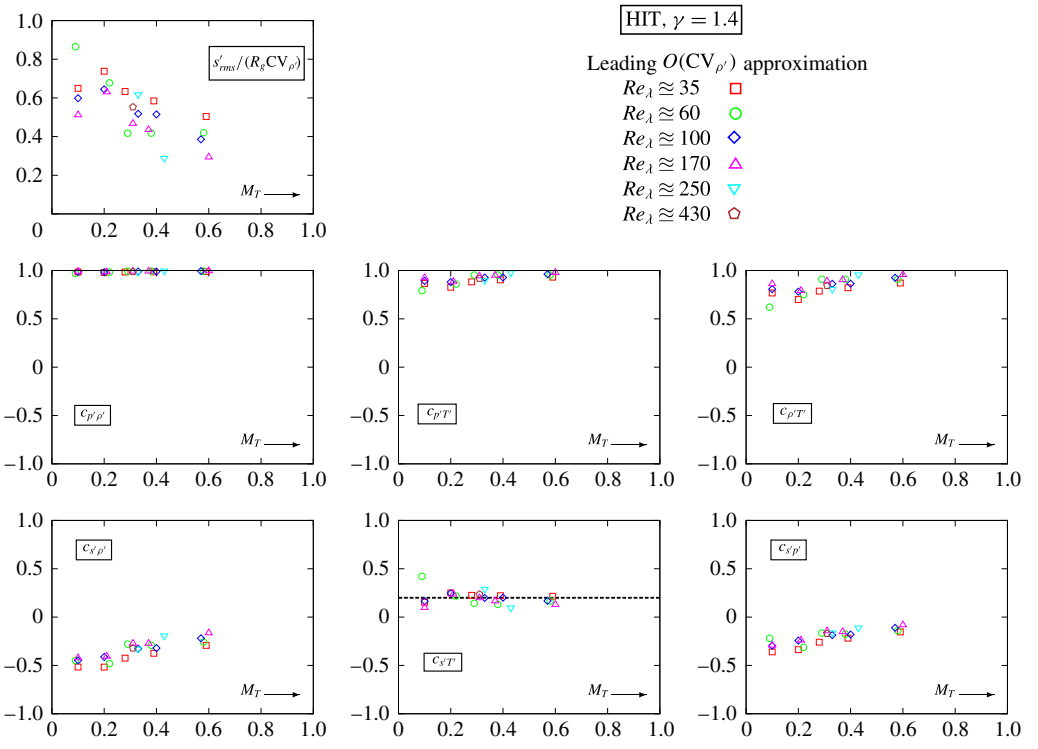

FIGURE 13. (Colour online) Leading-order estimates (4.5*a*), (4.3), (4.7) for $\{R_g^{-1}\,\mathrm{CV}_{\rho'}^{-1}\,s'_{rms}, c_{p'\rho'}, c_{p'T'}, c_{\rho'T'}, c_{s'\rho'}, c_{s'T'}, c_{s'p'}\}$ with input DNS data for $\{\mathrm{CV}_{\rho'}, \mathrm{CV}_{T'}, \mathrm{CV}_{p'}\}$ from sustained compressible HIT computations (Donzis & Jagannathan 2013; D. A. Donzis, 2016, Private communication; Jagannathan & Donzis 2016), for different values of $Re_\lambda \in [35, 430]$, plotted against the turbulent Mach number $M_T \in [0.1, 0.6]$.

satisfy $\mathrm{CV}_{T'} < \mathrm{CV}_{\rho'}$, except for a few near-wall channel data (figure 14), roughly corresponding to the peaks of $\mathrm{CV}_{\rho'}$ and $\mathrm{CV}_{T'}$ (Gerolymos & Vallet 2014, figure 5, p. 720) around $y^\star \approxeq 7$ where values $\mathrm{CV}_{\rho'} \approxeq \mathrm{CV}_{T'}$ are observed (figure 14). Simple calculations define zones on the $(\mathrm{CV}_{\rho'}^{-1}\,\mathrm{CV}_{T'},\ c_{\rho'T'})$-plane (figure 14) with specific orderings of the non-dimensional r.m.s. levels of thermodynamic fluctuations $\{\mathrm{CV}_{p'}, \mathrm{CV}_{\rho'}, \mathrm{CV}_{T'}, R_g^{-1}\,s'_{rms}\}$. For simplicity we study the case $\breve{\gamma} = 1.4$. Zone I at the bottom (figure 14), is characterized by low $\mathrm{CV}_{p'}$ compared to $\mathrm{CV}_{\rho'}$ and $\mathrm{CV}_{T'}$, contrary to the four other zones, which are essentially distinguished with respect to the relative importance of the non-dimensional entropy fluctuations. In zone I, $R_g^{-1}\,s'_{rms}$ is higher than $\{\mathrm{CV}_{\rho'}, \mathrm{CV}_{T'}, \mathrm{CV}_{p'}\}$, progressively diminishing through zones I–V. Zone V, where $R_g^{-1}\,s'_{rms} \lessapprox \mathrm{CV}_{T'} \lessapprox \mathrm{CV}_{\rho'} \lessapprox \mathrm{CV}_{p'}$ (figure 14), also contains the isolated point of isentropic turbulence, where

$$\left[s'_{rms} = 0 \overset{(2.1a)}{\Longleftrightarrow} s' = 0\,\forall\, t\right] \overset{(4.5b),\,(4.4)}{\Longleftrightarrow} \begin{cases} c_{\rho'T'} \approxeq +1 \\ \mathrm{CV}_{T'} \approxeq (\breve{\gamma} - 1)\,\mathrm{CV}_{\rho'} \\ \mathrm{CV}_{p'} \approxeq \breve{\gamma}\,\mathrm{CV}_{\rho'}. \end{cases} \tag{6.1}$$

Of course this is an inaccessible limit point, since it is highly improbable (impossible) for a turbulent flow to have $s' = 0\,\forall\, t$. Available DNS data for $\{\mathrm{CV}_{\rho'}^{-1}\,\mathrm{CV}_{T'},\ c_{\rho'T'}\}$

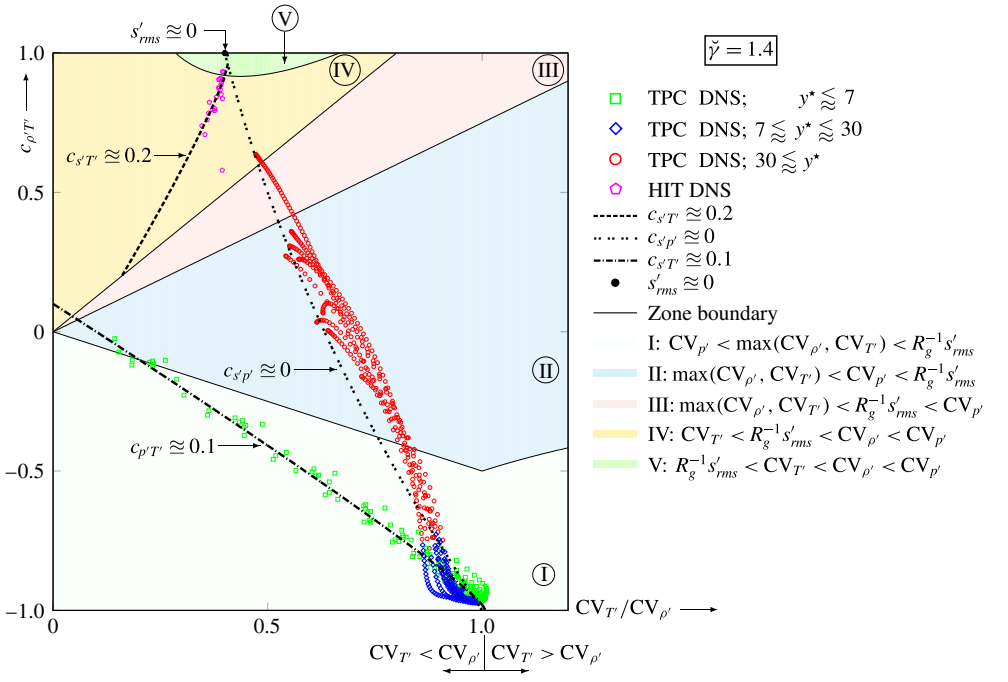

FIGURE 14. (Colour online) Map for $\breve{\gamma} = 1.4$ on the $(\mathrm{CV}_{\rho'}^{-1}\,\mathrm{CV}_{T'},\, c_{\rho'T'})$-plane of DNS data for compressible solenoidally forced sustained HIT (Donzis & Jagannathan 2013; D. A. Donzis, 2016, Private communication; Jagannathan & Donzis 2016, $0.1 \lessapprox M_T \lessapprox 0.6$, $35 \lessapprox Re_\lambda \lessapprox 430$) and for fully developed compressible turbulent plane channel (TPC) flow (Gerolymos & Vallet 2014, $0.35 \lessapprox \bar{M}_{CL} \lessapprox 2.48$, $78 \lessapprox Re_{\tau^\star} \lessapprox 341$), approximate (to leading order) loci of $[c_{s'p'} = 0]$ (6.4), of $[c_{s'T'} = 0.2]$ (6.2) and of $[c_{p'T'} = 0.1]$ (6.3), describing turbulence structure of specific flow regions, various zones (I to V; $\breve{\gamma} = 1.4$) corresponding to different orderings of the non-dimensional r.m.s. levels of thermodynamic fluctuations, and isolated point (within the leading-order approximate framework) of isentropic turbulence (6.1).

(Donzis & Jagannathan 2013; Gerolymos & Vallet 2014; D. A. Donzis, 2016, Private communication; Jagannathan & Donzis 2016) show that different flows or flow regions have specific thermodynamic turbulence structure (figure 14).

As already observed (figure 13) the HIT data follow (for the available $\gamma = 1.4$ computations) the $[c_{s'T'} \approx 0.2]$-line, which is easily calculated as

$$c_{\rho'T'} \overset{(4.5b),\,(4.6b)}{\approx} \left[\frac{1 - c_{s'T'}^2}{\breve{\gamma} - 1} \frac{\mathrm{CV}_{T'}}{\mathrm{CV}_{\rho'}} \pm c_{s'T'} \sqrt{1 - \frac{1 - c_{s'T'}^2}{(\breve{\gamma} - 1)^2} \left(\frac{\mathrm{CV}_{T'}}{\mathrm{CV}_{\rho'}} \right)^2} \right]_{(c_{s'T'}=0.2,\,\breve{\gamma}=1.4)} . \quad (6.2)$$

There is little scatter in the HIT DNS data (figure 14) except for one outlier corresponding to the $(Re_\lambda,\, M_T) \approx (60,\, 0.1)$ simulation (Donzis & Jagannathan 2013, table 1, p. 225). Mapping on the $(\mathrm{CV}_{\rho'}^{-1}\,\mathrm{CV}_{T'},\, c_{\rho'T'})$-plane explains why the alternative observation (figure 13) that the HIT data are also quite close to $c_{p'\rho'} \approx 1$ cannot be used, as it would erroneously imply by (4.3*a*), (4.4) $c_{\rho'T'} \approx 1$: in general approximations based on ± 1 values of correlation coefficients are singular as they invariably map by (4.3), (4.5), (4.6) to $|c_{\rho'T'}| \approx 1$.

The locus of the channel data depends on the non-dimensional wall distance $y^\star$ (3.2*b*,*c*). The near-wall points $y^\star \lessapprox 7$ seem to collapse onto a single curve. Observation of the correlation coefficients plotted against $y^\star$ suggests (figure 7) that in this region $c_{p'T'} \approxeq 0.1$ (for the available $\gamma = 1.4$ computations) $\forall\,(Re_{\tau\star}, \bar{M}_{CL})$. The appropriate branch of the $[c_{p'T'} \approxeq 0.1]$-line is determined by

$$c_{\rho'T'} \overset{(4.3b),\,(4.4)}{\approxeq} \left[-(1-c_{p'T'}^2)\,\frac{\mathrm{CV}_{T'}}{\mathrm{CV}_{\rho'}} + c_{p'T'}\sqrt{1-(1-c_{p'T'}^2)\left(\frac{\mathrm{CV}_{T'}}{\mathrm{CV}_{\rho'}}\right)^2}\right]_{(c_{p'T'}=0.1,\,\breve{\gamma}=1.4)} . \tag{6.3}$$

Although the mapping relation (6.3) does not involve $\breve{\gamma}$, it should be kept in mind that the observed value ($c_{p'T'} \approxeq 0.1$) was obtained from $[\gamma = 1.4]$-computations, and also that the wall is isothermal and cold with respect to the flow (Gerolymos & Vallet 2014, figure 1, p. 713). All available near-wall ($y^\star \lessapprox 7$) data follow the $[c_{p'T'} \approxeq 0.1]$-line with little scatter (figure 14).

In the region $7 \lessapprox y^\star \lessapprox 30$, roughly the lower buffer layer (Smits & Dussauge 2006, p. 203), suggests (figure 11) that $c_{s'p'} \approxeq 0$ (for the available $\gamma = 1.4$ computations), $\forall\,(Re_{\tau\star}, \bar{M}_{CL})$. Plotting the $[c_{s'p'} \approxeq 0]$-line, which is determined by

$$c_{\rho'T'} \overset{(A2b),\,(4.5b)}{\approxeq} \left[\frac{\breve{\gamma}-1}{2-\breve{\gamma}}\frac{\mathrm{CV}_{\rho'}}{\mathrm{CV}_{T'}} - \frac{1}{2-\breve{\gamma}}\frac{\mathrm{CV}_{T'}}{\mathrm{CV}_{\rho'}}\right]_{(c_{s'p'}=0,\,\breve{\gamma}=1.4)} \tag{6.4}$$

indicates good correlation of the data (figure 14). Notice that the data around $y^\star \approxeq 7$ correspond to a region around the point $[\mathrm{CV}_{\rho'} = \mathrm{CV}_{T'},\ c_{\rho'T'} = -1]$ where the $[c_{p'T'} \approxeq 0.1]$-line (6.3) crosses the $[c_{s'p'} \approxeq 0]$-line (6.4), both fitting the DNS data there (figure 14). DNS data for $y^\star \gtrapprox 30$ stay close (but not on) the $[c_{s'p'} \approxeq 0]$-line, and return to this locus near the centreline (figure 14), in line with the detailed plots of $c_{s'p'}$ versus $y^\star$ (figure 11).

The $(\mathrm{CV}_{\rho'}^{-1}\mathrm{CV}_{T'},\ c_{\rho'T'})$-plane, essentially inspired by (4.4) is not the only possible choice. The observation e.g. that sustained subsonic compressible HIT evolves with varying (M_T, Re_λ) along a $[c_{s'T'} \approxeq \text{const.}]$-line, and the corresponding model developed in § 7.1, suggest that mapping on the $(R_g^{-1}\mathrm{CV}_{\rho'}^{-1}s'_{rms},\ c_{s'T})$ is an alternative choice. In general, any couple of parameters in the set TTS (1.2) can potentially be used to define the mapping plane: by (4.3), (4.4), (4.5), (4.7) the set TTS (1.2) has, to leading order, 2 degrees-of-freedom.

7. Applications

The representations of compressible turbulence in the $(\mathrm{CV}_{\rho'}^{-1}\mathrm{CV}_{T'},\ c_{\rho'T'})$-plane (CT-map) were found very useful in identifying the behaviour of the thermodynamic fluctuations and of their correlations for different flows or different flow regions (figure 14). Examples of applications are the development of a simple model for thermodynamic turbulence structure of sustained compressible HIT (§ 7.1) and the $[c_{s'p'} \approxeq 0]$-approximation in the lower buffer region ($7 \lessapprox y^\star \lessapprox 40$) in compressible wall turbulence (§ 7.2).

7.1. *Thermodynamic turbulence structure in sustained subsonic HIT*

It appears from DNS data (Donzis & Jagannathan 2013; D. A. Donzis, 2016, Private communication; Jagannathan & Donzis 2016) that, as M_T increases, compressible

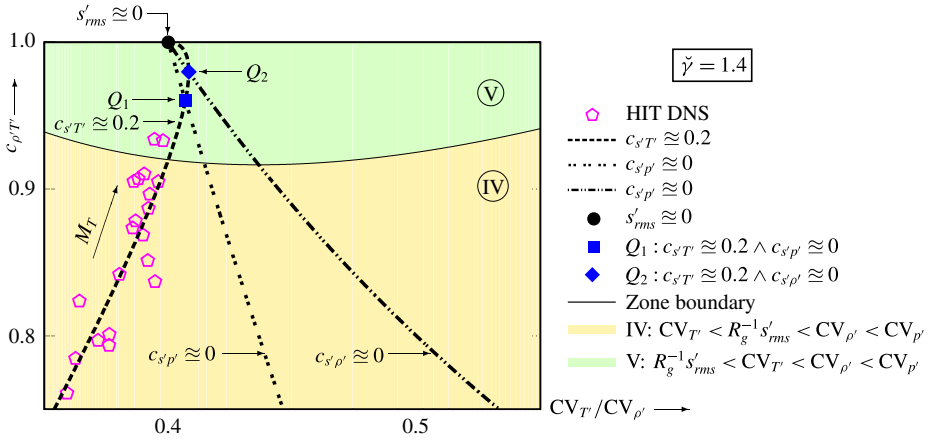

FIGURE 15. (Colour online) Zoom on the $(\mathrm{CV}_{\rho'}^{-1}\,\mathrm{CV}_{T'},\ c_{\rho'T'})$-plane of DNS data for compressible solenoidally forced sustained HIT (Donzis & Jagannathan 2013; D. A. Donzis, 2016, Private communication; Jagannathan & Donzis 2016, $0.1 \approxeq M_T \approxeq 0.6$, $35 \approxeq Re_\lambda \approxeq 430$) following the approximation (to leading order) of the $[c_{s'T'} = 0.2]$-locus (6.2), which intersects the $[c_{s'T'} = 0]$-locus (6.4) at point Q_1 and the $[c_{s'\rho'} = 0]$-locus at point Q_2, and finally passes through the isolated limit point (within the leading-order approximate framework) of isentropic turbulence (6.1).

subsonic HIT thermodynamic turbulence structure parameters (1.2) tend to a slowly varying state (figures 2, 12, 8, 13) with a Re_λ-dependency, which is clearly visible e.g. in the evolution of $c_{\rho'T'}$ versus M_T (figure 12) and even more so for $R_g^{-1}\,\mathrm{CV}_{\rho'}^{-1}\,s'_{rms}$ versus M_T (figure 13). However, when considering relations between elements of the set TTS (1.2) only, such as mapping on the $(\mathrm{CV}_{\rho'}^{-1}\,\mathrm{CV}_{T'},\ c_{\rho'T'})$-plane (figure 14), the DNS data collapse with little scatter on a single curve, following the $[c_{s'T'} = 0.2]$-locus (6.2), this value corresponding to the available $\gamma = 1.4$ DNS data (Donzis & Jagannathan 2013; D. A. Donzis, 2016, Private communication; Jagannathan & Donzis 2016). Zoom on the HIT data in the $(\mathrm{CV}_{\rho'}^{-1}\,\mathrm{CV}_{T'},\ c_{\rho'T'})$-plane (figure 15) confirms that there is little scatter. The DNS data follow the $\ominus$-branch of the $[c_{s'T'} = 0.2]$-line (6.2) up to, approximately, its intersection with the $[R_g^{-1}\,s'_{rms} = \mathrm{CV}_{T'}]$-locus which defines the boundary between zones IV and V. The $\ominus$-branch of the $[c_{s'T'} = 0.2]$-line (6.2) terminates (figure 15) at point Q_2 where $c_{s'\rho'} = 0$. It is then continued (figure 15) by the $\oplus$-branch of the $[c_{s'T'} = 0.2]$-line (6.2), which passes through the $[s'_{rms} = 0]$-point (6.1). Increasing M_T corresponds to decreasing $R_g^{-1}\,s'_{rms}$ (figure 13), i.e. increasing $c_{\rho'T'}$ along the $[c_{s'T'} = 0.2]$-line. Before reaching point Q_2, the $[c_{s'T'} = 0.2]$-line intersects (figure 15) the $[c_{s'p'} = 0]$-line (6.4) at point Q_1. It is unclear how the evolution of HIT continues with increasing M_T, since we expect that shocklets and shocks for supersonic $M_T > 1$ (Wang *et al.* 2011) will increase entropy production and substantially modify the thermodynamic turbulence structure (1.2). DNS data for higher M_T are required to resolve this issue. We concentrate here on subsonic $M_T < 1$ HIT (Donzis & Jagannathan 2013; D. A. Donzis, 2016, Private communication; Jagannathan & Donzis 2016).

We defer for the moment the quest of a $(Re_\lambda,\ M_T)$-correlation of the data and concentrate instead on thermodynamic fluctuations. The data on the $(\mathrm{CV}_{\rho'}^{-1}\,\mathrm{CV}_{T'},\ c_{\rho'T'})$-plane, along the $[c_{s'T'} = 0.2]$-line (figures 14, 15) show that $\mathrm{CV}_{\rho'}^{-1}\,\mathrm{CV}_{T'}$ varies

little with M_T, contrary to $R_g^{-1}\,\mathrm{CV}_{\rho'}^{-1}\,s'_{rms}$ (figure 13). Therefore, $R_g^{-1}\,\mathrm{CV}_{\rho'}^{-1}\,s'_{rms}$ is an appropriate structure parameter to be used as independent variable in describing thermodynamic turbulence (1.2), along with the constraint that $c_{s'T'}=\text{const.}$ ($\approxeq 0.2$ for $\gamma=1.4$), which is tantamount to mapping the elements of the set TTS (1.2) on the $(R_g^{-1}\,\mathrm{CV}_{\rho'}^{-1}\,s'_{rms},\,c_{s'T'})$-plane. Straightforward calculations yield the following model

$$\breve{\gamma}=1.4 \implies c_{s'T'}\approxeq 0.2, \tag{7.1a}$$

$$\frac{\mathrm{CV}_{T'}}{\mathrm{CV}_{\rho'}} \overset{(4.6b),\,(4.5b)}{\approxeq} \left[(\breve{\gamma}-1)\left(c_{s'T'}\frac{s'_{rms}}{R_g\,\mathrm{CV}_{\rho'}}+\sqrt{1-(1-c_{s'T'}^2)\left(\frac{s'_{rms}}{R_g\,\mathrm{CV}_{\rho'}}\right)^2}\right)\right]_{(7.1a)}, \tag{7.1b}$$

$$c_{\rho'T'} \overset{(4.6b)}{\approxeq} \left[\sqrt{1-(1-c_{s'T'}^2)\left(\frac{s'_{rms}}{R_g\,\mathrm{CV}_{\rho'}}\right)^2}\right]_{(7.1a)}. \tag{7.1c}$$

Actually (7.1) maps the $(R_g^{-1}\,\mathrm{CV}_{\rho'}^{-1}\,s'_{rms},\,c_{s'T'})$-plane onto the $(\mathrm{CV}_{\rho'}^{-1}\,\mathrm{CV}_{T'},\,c_{\rho'T'})$-plane. We can therefore readily compute $\mathrm{CV}_{\rho'}^{-1}\,\mathrm{CV}_{p'}$ by (4.4), and complete the model by the previously worked out leading $O(\mathrm{CV}_{\rho'})$ approximations, e.g.

$$\frac{\mathrm{CV}_{p'}}{\mathrm{CV}_{\rho'}}\approxeq (4.4)\big|_{(7.1)}, \tag{7.2a}$$

$$c_{p'\rho'}\approxeq (4.3a)\big|_{(7.1),\,(7.2a)}, \tag{7.2b}$$

$$c_{p'T'}\approxeq (4.3b)\big|_{(7.1),\,(7.2a)}, \tag{7.2c}$$

$$c_{s'\rho'}\approxeq (4.7a)\big|_{(7.1),\,(7.2a)}, \tag{7.2d}$$

$$c_{s'p'}\approxeq (4.7c)\big|_{(7.1),\,(7.2a)}. \tag{7.2e}$$

The proposed correlations (7.1), (7.2), represent the elements of the set TTS (1.2) for subsonic sustained HIT as a function of the structure parameter $R_g^{-1}\,\mathrm{CV}_{\rho'}^{-1}\,s'_{rms}$. DNS data follow closely the proposed $[c_{s'T'}=0.2]$-model (figure 16), with very little scatter, removing the strong Re_λ-dependency observed when using M_T as independent variable (figure 13). Even the minute variation of $c_{p'\rho'}$ is captured by the model with very little scatter (figure 16). The model is inherently parametrized by $\breve{\gamma}$ through the constant $c_{s'T'}(\breve{\gamma})$. DNS computations with different values of γ are necessary to determine the functional dependence $c_{s'T'}(\breve{\gamma})$. Further work is also necessary to correlate the single relevant thermodynamic structure parameter $R_g^{-1}\,\mathrm{CV}_{\rho'}^{-1}\,s'_{rms}$ with (Re_λ, M_T).

7.2. *The* $[c_{s'p'}\approxeq 0]$*-approximation in compressible wall turbulence*

Comparison (figures 6, 7, 11) with compressible channel DNS data (Gerolymos & Vallet 2014) indicates that the leading $O(\mathrm{CV}_{\rho'})$ approximations (4.3*a*), (4.3*b*), (4.7*c*) for the correlation coefficients involving p', $\{c_{p'\rho'},\,c_{p'T'},\,c_{s'p'}\}$, become, progressively with increasing $\bar{M}_{CL}\gtrapprox 2$, inaccurate in the region $10\lessapprox y^\star\lessapprox 40$. Furthermore, it was shown that higher $O(\mathrm{CV}_{\rho'}^2)$ expansions for the correlation coefficients $c_{p'\rho'}$ (4.2*a*) and $c_{p'T'}$ (4.2*b*), which require DNS data for the 3CCs $c_{\rho'T'T'}$ and $c_{\rho'\rho'T'}$, are in excellent agreement with DNS data (figures 6, 7), identifying the $O(\mathrm{CV}_{\rho'}^2)$ terms to be responsible for the observed discrepancies. Therefore, if we need to approximate

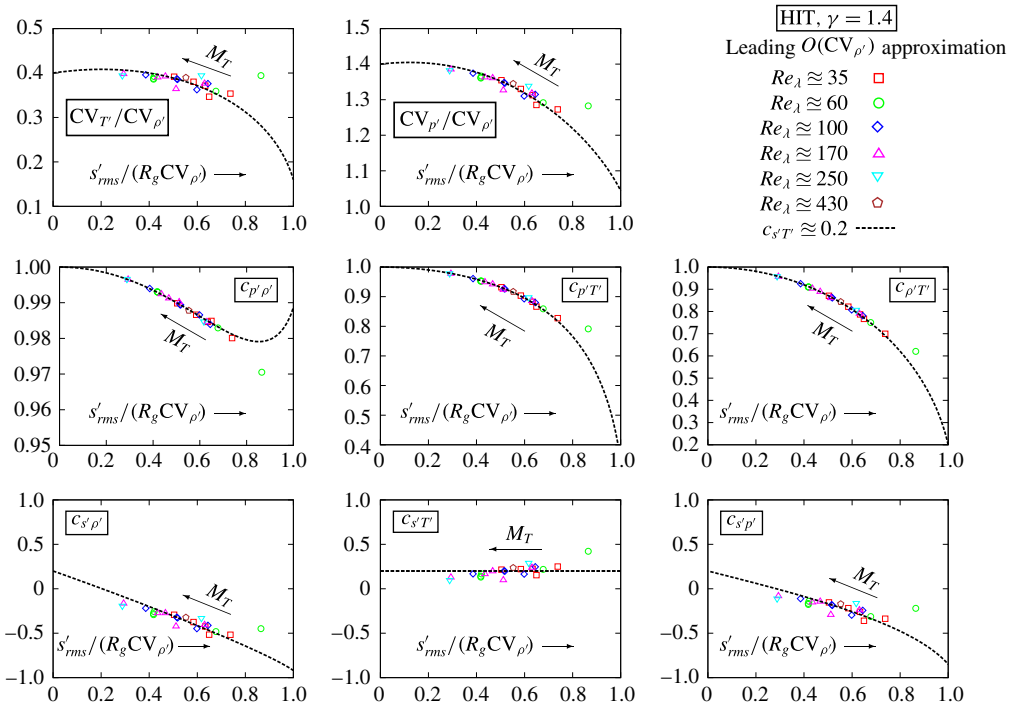

FIGURE 16. (Colour online) Predictions of the $[c_{s'T'} = 0.2]$-model (7.1), (7.2) representing thermodynamic turbulence structure (1.2) of sustained solenoidally forced subsonic aerodynamic ($\gamma = 1.4$) HIT as a unique function of the structure parameter $R_g^{-1}\,\mathrm{CV}_{\rho'}^{-1}\,s'_{rms}$, compared with leading-order estimates (4.5*a*), (4.3), (4.7) with input DNS data for $\{\mathrm{CV}_{\rho'},\ \mathrm{CV}_{T'},\ \mathrm{CV}_{p'}\}$ (Donzis & Jagannathan 2013; D. A. Donzis, 2016, Private communication; Jagannathan & Donzis 2016, $0.1 \lessapprox M_T \lessapprox 0.6$, $35 \lessapprox Re_\lambda \lessapprox 430$).

$\{c_{p'\rho'},\ c_{p'T'},\ c_{s'p'}\}$ with inputs only $\{\mathrm{CV}_{\rho'},\ \mathrm{CV}_{T'},\ \mathrm{CV}_{p'}\}$, improvement of the $O(\mathrm{CV}_{\rho'})$ approximations (4.3*a*), (4.3*b*), (4.7*c*) in the region of discrepancy ($10 \lessapprox y^\star \lessapprox 40$) and at high $\bar{M}_{CL}$, is desirable. The mapping on the $(\mathrm{CV}_{\rho'}^{-1}\,\mathrm{CV}_{T'},\ c_{\rho'T'})$-plane (figure 14) revealed (§ 6) that precisely in that region DNS data follow the $[c_{s'p'} = 0]$-line, and this is confirmed by the plots (figures 6, 7, (1.2)) of $c_{s'p'}$ versus $y^\star\ \forall\,(Re_{\tau^\star}, \bar{M}_{CL})$. Further away from the wall, the DNS data show that $c_{s'p'}$ slightly increases and then returns to 0 near the centreline (figures 6, 7, (1.2), 14). It seemed therefore worthwhile to check whether a $[c_{s'p'} = 0]$-approximation (with unique inputs $\{\mathrm{CV}_{\rho'}, \mathrm{CV}_{T'}, \mathrm{CV}_{p'}\}$) can reduce the aforementioned discrepancies. Simple leading-order calculations yield

$$c_{s'p'} = 0 \overset{(\mathrm{A}2a),\,(4.2a)}{\Longrightarrow} \begin{cases} c_{p'\rho'} \approxeq \dfrac{1}{\breve{\gamma}}\dfrac{\mathrm{CV}_{p'}}{\mathrm{CV}_{\rho'}} \\ c_{p'T'} \approxeq \dfrac{\breve{\gamma}-1}{\breve{\gamma}}\dfrac{\mathrm{CV}_{p'}}{\mathrm{CV}_{T'}} \\ c_{s'p'} \approxeq 0. \end{cases} \tag{7.3}$$

Comparison of the $[c_{s'p'} = 0]$-approximation (7.3) with the leading $O(\mathrm{CV}_{\rho'})$ approximations (4.3*a*), (4.3*b*), (4.7*c*) and DNS data for supersonic channel flows (figure 17), show that (7.3) is a good approximation $\forall\, y^\star \gtrapprox 7$, particularly in the region $10 \lessapprox y^\star \lessapprox 40$

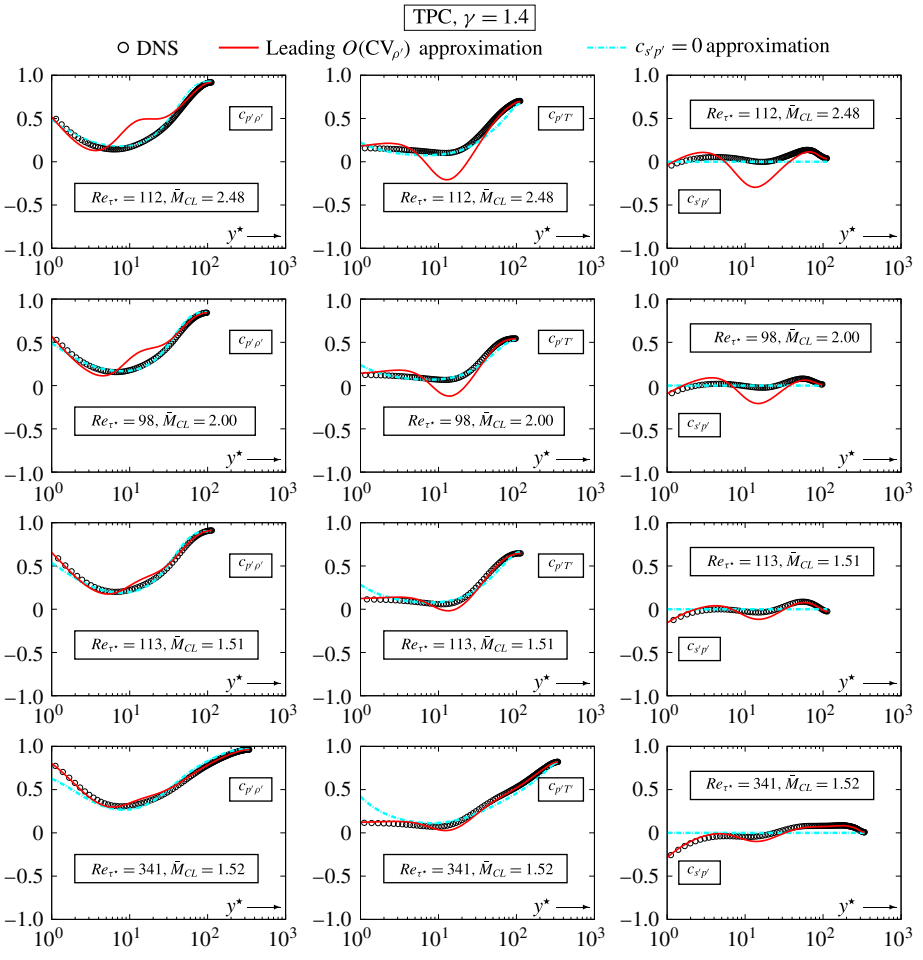

FIGURE 17. (Colour online) Comparison of the leading $O(\mathrm{CV}_{\rho'})$ approximations (4.3*a*), (4.3*b*) (4.7*c*) of $c_{p'\rho'}(\mathrm{CV}_{\rho'}, \mathrm{CV}_{T'}, \mathrm{CV}_{p'})$, of $c_{p'T'}(\mathrm{CV}_{\rho'}, \mathrm{CV}_{T'}, \mathrm{CV}_{p'})$ and of $c_{s'p'}(\mathrm{CV}_{\rho'}, \mathrm{CV}_{T'}, \mathrm{CV}_{p'})$, with the $[c_{s'p'} = 0]$-approximations (7.3) and with DNS data for supersonic compressible fully developed turbulent plane channel (TPC) flow (Gerolymos & Vallet 2014, $1.50 \lessapprox \bar{M}_{CL} \lessapprox 2.48$, $98 \lessapprox Re_{\tau\star} \lessapprox 341$), plotted against the HCB-scaled wall distance $y^\star$ (3.2*b*,*c*).

where the leading $O(\mathrm{CV}_{\rho'})$ approximations are not satisfactory when $\bar{M}_{CL} \gtrapprox 2$. We may therefore construct a composite C^0-continuous approximation using for supersonic $\bar{M}_{CL} > 1$, the $[c_{s'p'} = 0]$-approximation (7.3) in the interval between the two 0-crossing points around the global negative minimum of the leading $O(\mathrm{CV}_{\rho'})$ approximation of $c_{s'p'}$ (figure 17), and the $O(\mathrm{CV}_{\rho'})$ approximations (4.3*a*), (4.3*b*), (4.7*c*) elsewhere. For subsonic $\bar{M}_{CL} < 1$ flows the $O(\mathrm{CV}_{\rho'})$ approximations are excellent and require no modification.

8. Conclusions

In turbulent flows of a working medium following the perfect-gas equation of state, the coefficients of variation of the basic thermodynamic variables $\{\mathrm{CV}_{\rho'}, \mathrm{CV}_{T'}, \mathrm{CV}_{p'}\}$

strongly increase with the characteristic flow Mach number, and so do the non-dimensional entropy fluctuations $R_g^{-1}\, s'_{rms}$. These non-dimensional gauges of the thermodynamic fluctuations level $\{\mathrm{CV}_{\rho'},\ \mathrm{CV}_{T'},\ \mathrm{CV}_{p'},\ R_g^{-1}\, s'_{rms}\}$ are invariably of the same order of magnitude at a given point of the flow. Therefore the notion of strongly or mildly compressible turbulence defined in terms of the level of $\mathrm{CV}_{\rho'}$ actually concerns all of these quantities simultaneously.

As a consequence of the equation of state, exact relations can be worked out between correlation coefficients involving $\{\rho', T', p'\}$ for moments of any order. These exact relations can be expanded in power series of the coefficients of variation (assumed <1). Regarding entropy, fluctuations s' can be expressed as power series of $\{\rho', T', p'\}$. In particular the influence of variable $c_p(T)$ thermodynamics on s' is quadratic ($\propto T'^2$), and therefore does not appear in leading-order approximations.

Leading-order approximations, $O(\mathrm{CV}_{\rho'}^2)$ for the entropy variance $R_g^{-1}\, s'_{rms}$ and $O(\mathrm{CV}_{\rho'})$ for the correlation coefficients between thermodynamic variables $\{s', \rho', T', p'\}$, with inputs $\{\mathrm{CV}_{p'}, \mathrm{CV}_{\rho'}, \mathrm{CV}_{T'}\}$, are developed and compare with excellent accuracy with DNS data for HIT ($M_T \lessapprox 0.6$) and channel flow ($\bar{M}_{CL} \lessapprox 2.5$), except for those involving p' at high $\bar{M}_{CL} \gtrapprox 2$ which show discrepancies in the lower buffer layer ($10 \lessapprox y^\star \lessapprox 40$). The $O(\mathrm{CV}_{\rho'}^2)$ terms of the asymptotic expansions of $c_{p'\rho'}$ and $c_{p'T'}$ were evaluated using DNS data and shown to correct for these discrepancies.

The contradictory values of the polytropic exponent estimates $n_P(\mathrm{CV}_{p'}, \mathrm{CV}_{\rho'})$ and $n_P(\mathrm{CV}_{\rho'}, \mathrm{CV}_{T'})$ in channel flow demonstrate that near-wall turbulence is strongly non-isentropic and, furthermore, that it cannot be approximated as a polytropic process. Indeed we show the more general result that, to leading order, turbulence cannot be approximated as a polytropic process unless $c_{\rho'T'} \approxeq +1$, whereas near the wall $c_{\rho'T'} < 0$.

The thermodynamic turbulence structure (ratios of non-dimensional variances and correlation coefficients), $\mathrm{TTS} := \{R_g^{-1}\, \mathrm{CV}_{\rho'}^{-1}\, s'_{rms}, \mathrm{CV}_{\rho'}^{-1}\, \mathrm{CV}_{T'}, \mathrm{CV}_{\rho'}^{-1}\, \mathrm{CV}_{p'}, c_{p'\rho'}, c_{p'T'}, c_{\rho'T'}, c_{s'\rho'}, c_{s'T'}, c_{s'p'}\}$, within the range of validity of the leading $O(\mathrm{CV}_{\rho'})$ approximations, has only 2 independent parameters and can therefore be represented e.g. on the $(\mathrm{CV}_{\rho'}^{-1}\, \mathrm{CV}_{T'},\ c_{\rho'T'})$-plane. Plotting on this plane DNS data and mapping isolines of the other thermodynamic turbulence structure parameters is useful in identifying and analysing different flows or flow regions. We show in particular that subsonic sustained HIT is characterized by $c_{s'T'} \approxeq$ const., and that channel flow follows $c_{p'T'} \approxeq$ const. very near the wall ($y^\star \lessapprox 7$) then switching to $c_{s'p'} \approxeq 0$ further away from the wall ($y^\star \gtrapprox 7$). These observations were used to correlate subsonic HIT data as a function of the single structure parameter $R_g^{-1}\, \mathrm{CV}_{\rho'}^{-1}\, s'_{rms}$ and to develop for channel flow a composite approximation which corrects the aforementioned discrepancies for the p' correlations at high $\bar{M}_{CL} \gtrapprox 2$.

DNS data clearly show that thermodynamic turbulence structure for a given flow is only weakly dependent on the relevant Mach number, and that no particular structure modification is observed as the quasi-incompressible limit is approached. This is also the case of $c_{\rho'T'}$ which, therefore, is in not an indicator of compressibility: it controls instead the relative importance of $\mathrm{CV}_{p'}^2$ compared to $\mathrm{CV}_{\rho'}^2 + \mathrm{CV}_{T'}^2$.

There are several perspectives for future work:

(i) study of the thermodynamic turbulence signature of various other basic flows on the $(\mathrm{CV}_{\rho'}^{-1}\, \mathrm{CV}_{T'},\ c_{\rho'T'})$-plane;

(ii) determination by new DNS computations of the $c_{s'T'}(\breve{\gamma})$-dependency in subsonic HIT and correlation of the structure parameter $R_g^{-1}\, \mathrm{CV}_{\rho'}^{-1}\, s'_{rms}$ with (Re_λ, M_T) as well as study of higher M'_{rms};

(iii) application of the relations and approximations developed in the present work to analogies between transport correlation coefficients $c_{(\cdot)'u'_i}$.

Acknowledgements

The authors are listed alphabetically. We are particularly grateful to Professor D. Donzis for providing the HIT DNS data (D. A. Donzis, 2016, Private communication) used in the paper. The computations reported in the present work were performed using HPC resources allocated at GENCI–IDRIS (Grant 2015–022139) and at ICS–UPMC (ANR–10–EQPX–29–01). Tabulated DNS data are available at http://www.aerodynamics.fr/DNS_database/CT_chnnl. The present work was partly supported by the ANR project NumERICCS (ANR–15–CE06–0009).

Appendix A. Three-moment correlation coefficients

We use in the paper three approximate relations involving 3-moment correlation coefficients. Multiplying (2.4) by $\rho'T'$ yields upon averaging and using definitions (2.1), (2.3)

$$c_{p'\rho'T'} \sim \underbrace{c_{\rho'\rho'T'}\frac{\mathrm{CV}_{\rho'}}{\mathrm{CV}_{p'}}+c_{\rho'T'T'}\frac{\mathrm{CV}_{T'}}{\mathrm{CV}_{p'}}}_{\overset{(2.2)}{=}O(1)}+\underbrace{(c_{\rho'\rho'T'T'}-c^2_{\rho'T'})\frac{\mathrm{CV}_{\rho'}\,\mathrm{CV}_{T'}}{\mathrm{CV}_{p'}}}_{\overset{(2.2)}{=}O(\mathrm{CV}_{\rho'})}+\underbrace{O(\mathrm{CV}_{\rho'}\,\mathrm{CV}_{T'})}_{\overset{(2.2)}{=}O(\mathrm{CV}^2_{\rho'})}, \tag{A 1a}$$

where (2.2) is used to formally identify the order of magnitude of different terms in (A 1*a*) with some power of $\mathrm{CV}_{\rho'}$. Multiplying (2.4) by $T'p'$, $p'\rho'$, $\rho'\rho'$, $T'T'$ or $p'p'$, yields in the same way five other relations between 3-moment correlation coefficients. Combining these relations with (A 1*a*) yields after some algebra the alternative approximate relation for $c_{p'\rho'T'}$

$$c_{p'\rho'T'} \approxeq -\frac{1}{3}S_{T'}\frac{\mathrm{CV}^2_{T'}}{\mathrm{CV}_{p'}\mathrm{CV}_{\rho'}}-\frac{1}{3}S_{\rho'}\frac{\mathrm{CV}^2_{\rho'}}{\mathrm{CV}_{p'}\mathrm{CV}_{T'}}+\frac{1}{3}S_{p'}\frac{\mathrm{CV}^2_{p'}}{\mathrm{CV}_{\rho'}\mathrm{CV}_{T'}}+O(\mathrm{CV}_{\rho'}). \tag{A 1b}$$

Multiplying (2.8*b*) by $T'T'$ yields upon averaging and using definitions (2.1), (2.3).

$$c_{s'T'T'}\frac{s'_{rms}}{R_g} \sim \frac{1}{\breve{\gamma}-1}S_{T'}\,\mathrm{CV}_{T'}-c_{\rho'T'T'}\,\mathrm{CV}_{\rho'}+O\left(\mathrm{CV}^2_{\rho'},\mathrm{CV}^2_{T'}\right). \tag{A 1c}$$

Multiplying (2.8) by p', averaging and introducing definitions (2.1), (2.3) readily yields

$$\begin{aligned} c_{s'p'}\frac{s'_{rms}}{R_g} &\sim \frac{\breve{\gamma}}{\breve{\gamma}-1}\left(c_{p'T'}\,\mathrm{CV}_{T'}-\frac{1}{2}c_{p'T'T'}\,\mathrm{CV}^2_{T'}\right)-\left(\mathrm{CV}_{p'}-\frac{1}{2}S_{p'}\,\mathrm{CV}^2_{p'}\right)\\ &\quad+\frac{1}{2}c_{p'T'T'}\mathrm{CV}^2_{T'}\frac{\bar{T}}{R_g}\left.\frac{\mathrm{d}c_p}{\mathrm{d}T}\right|_{\bar{T}}+O(\mathrm{CV}^3_{p'},\mathrm{CV}^3_{T'}) \qquad \text{(A 2a)}\\ &\sim \frac{1}{\breve{\gamma}-1}\left(c_{p'T'}\,\mathrm{CV}_{T'}-\frac{1}{2}c_{p'T'T'}\,\mathrm{CV}^2_{T'}\right)-\left(c_{p'\rho'}\,\mathrm{CV}_{\rho'}-\frac{1}{2}c_{p'\rho'\rho'}\,\mathrm{CV}^2_{\rho'}\right)\\ &\quad+\frac{1}{2}c_{p'T'T'}\mathrm{CV}^2_{T'}\frac{\bar{T}}{R_g}\left.\frac{\mathrm{d}c_p}{\mathrm{d}T}\right|_{\bar{T}}+O(\mathrm{CV}^3_{\rho'},\mathrm{CV}^3_{T'}) \qquad \text{(A 2b)}\end{aligned}$$

used in the development of the $[c_{s'p'}\approxeq 0]$-approximation § 7.2.

REFERENCES

BANERJEE, S. & GALTIER, S. 2014 A Kolomogorov-like exact relation for compressible polytropic turbulence. *J. Fluid Mech.* **542**, 230–242.

BARRE, S. & BONNET, J. P. 2015 Detailed experimental study of a highly compressible supersonic turbulent plane mixing layer and comparison with most recent DNS results: 'towards an accurate description of compressibility effects in supersonic free shear flows'. *Intl J. Heat Fluid Flow* **51**, 324–334.

BLAISDELL, G. A., MANSOUR, N. N. & REYNOLDS, W. C. 1993 Compressibility effects on the growth and structure of homogeneous turbulent shear flow. *J. Fluid Mech.* **256**, 443–485.

BRADSHAW, P. 1977 Compressible turbulent shear layers. *Annu. Rev. Fluid Mech.* **9**, 33–54.

CHU, B. T. & KOVÁSZNAY, L. S. G. 1958 Nonlinear interactions in a viscous heat-conducting compressible gas. *J. Fluid Mech.* **3**, 494–514.

COLEMAN, G. N., KIM, J. & MOSER, R. D. 1995 A numerical study of turbulent supersonic isothermal-wall channel flow. *J. Fluid Mech.* **305**, 159–183.

DONZIS, D. A. & JAGANNATHAN, S. 2013 Fluctuation of thermodynamic variables in stationary compressible turbulence. *J. Fluid Mech.* **733**, 221–244.

DUAN, L., CHOUDHARI, M. M. & ZHANG, C. 2016 Pressure fluctuations induced by a hypersonic turbulent boundary-layer. *J. Fluid Mech.* **804**, 578–607.

DUAN, L. & MARTÍN, M. P. 2011 Direct numerical simulation of hypersonic turbulent boundary-layers. Part 4. Effect of high enthalpy. *J. Fluid Mech.* **684**, 25–59.

ESWARAN, V. & POPE, S. B. 1988 An examination of forcing in DNS of turbulence. *Comput. Fluids* **16** (3), 257–278.

FOYSI, H., SARKAR, S. & FRIEDRICH, R. 2004 Compressibility effects and turbulence scalings in supersonic channel flow. *J. Fluid Mech.* **509**, 207–216.

GATSKI, T. B. & BONNET, J.-P. 2009 *Compressibility, Turbulence and High Speed Flow*. Elsevier.

GEROLYMOS, G. A., SÉNÉCHAL, D. & VALLET, I. 2010 Performance of very-high-order upwind schemes for DNS of compressible wall-turbulence. *Intl J. Numer. Meth. Fluids* **63**, 769–810.

GEROLYMOS, G. A., SÉNÉCHAL, D. & VALLET, I. 2013 Wall effects on pressure fluctuations in turbulent channel flow. *J. Fluid Mech.* **720**, 15–65.

GEROLYMOS, G. A. & VALLET, I. 1996 Implicit computation of the 3-D compressible Navier–Stokes equations using $k-\varepsilon$ turbulence closure. *AIAA J.* **34** (7), 1321–1330.

GEROLYMOS, G. A. & VALLET, I. 2014 Pressure, density, temperature and entropy fluctuations in compressible turbulent plane channel flow. *J. Fluid Mech.* **757**, 701–746.

GUARINI, S. E., MOSER, R. D., SHARIFF, K. & WRAY, A. 2000 Direct numerical simulation of a supersonic turbulent boundary-layer at Mach 2.5. *J. Fluid Mech.* **414**, 1–33.

HANSEN, C. F. 1958 Approximations for the thermodynamic and transport properties of high-temperature air. *Tech. Note* 4150. NACA, Ames Aeronautical Laboratory, Moffett Field, CA, USA.

HUANG, P. G., COLEMAN, G. N. & BRADSHAW, P. 1995 Compressible turbulent channel flows: DNS results and modelling. *J. Fluid Mech.* **305**, 185–218.

JAGANNATHAN, S. & DONZIS, D. A. 2016 Reynolds and mach number scaling in solenoidally-forced compressible turbulence using high-resolution direct numerical simulations. *J. Fluid Mech.* **789**, 669–707.

KIM, J. 1989 On the structure of pressure fluctuations in simulated turbulent channel-flow. *J. Fluid Mech.* **205**, 421–451.

KISTLER, A. L. 1959 Fluctuation measurements in a supersonic turbulent boundary-layer. *Phys. Fluids* **2**, 290–297.

KOVÁSZNAY, L. S. G. 1953 Turbulence in supersonic flow. *J. Aero. Sci.* **20**, 657–674; 682.

LADERMAN, A. J. & DEMETRIADES, A. 1974 Mean and fluctuating flow measurements in the hypersonic boundary-layer over a cooled wall. *J. Fluid Mech.* **63**, 121–144.

LAGHA, M., KIM, J., ELDREDGE, J. D. & ZHONG, X. 2011 Near-wall dynamics of compressible boundary layers. *Phys. Fluids* **23**, 065109(1–13).

LECHNER, R., SESTERHENN, J. & FRIEDRICH, R. 2001 Turbulent supersonic channel flow. *J. Turbul.* **2**, 001.1–25.

LEE, S., LELE, S. K. & MOIN, P. 1991 Eddy shocklets in decaying compressible turbulence. *Phys. Fluids* A **3** (4), 657–664.

LELE, S. K. 1994 Compressibility effects on turbulence. *Annu. Rev. Fluid Mech.* **26**, 211–254.

LIEPMANN, H. W. & ROSHKO, A. 1957 *Elements of Gasdynamics*. John Wiley.

MAHESH, K., LELE, S. K. & MOIN, P. 1997 The influence of entropy fluctutions on the interaction of turbulence with a shock-wave. *J. Fluid Mech.* **334**, 353–379.

MODESTI, D. & PIROZZOLI, S. 2016 Reynolds and Mach number effects in compressible turbulent channel. *Intl J. Heat Fluid Flow* **59** (33–49).

MORKOVIN, M. V. 1962 Effects of compressibility on turbulent flows. In *Mechanics of Turbulence (Proceedings of the International Colloquium, Aug. 28–Sep. 2, 1961, Marseille, [Fra])* (ed. A. Favre), Colloques Internationaux du CNRS 108, pp. 367–380. Editions du CNRS.

PANTANO, C. & SARKAR, S. 2002 A study of compressibility effects in the high-speed turbulent shear layer using direct simulation. *J. Fluid Mech.* **451**, 329–371.

PHAM, H. (Ed.) 2006 *Handbook of Engineering Statistics*. Springer.

RISTORCELLI, J. R. 1997 A pseudosound constitutive relationship for the dilatational covariances in compressible turbulence. *J. Fluid Mech.* **347**, 37–70.

RUBESIN, M. W. 1976 A 1-equation model of turbulence for use with the compressible Navier–Stokes equations. *Tech. Mem.* NASA–1976–TM–X–73128. NASA, Ames Research Center, Moffett Field, CA, USA.

SARKAR, S. 1995 The stabilizing effect of compressibility in turbulent shear flow. *J. Fluid Mech.* **282**, 163–186.

SHADLOO, M. S., HADJADJ, A. & HUSSAIN, F. 2015 Statistical behavior of supersonic turbulent boundary layers with heat transfer at $m_\infty = 2$. *Intl J. Heat Fluid Flow* **53**, 113–134.

SMITS, A. J. & DUSSAUGE, J. P. 2006 *Turbulent Shear Layers in Supersonic Flow*. Springer.

SUMAN, S. & GIRIMAJI, S. S. 2001 Dynamical model for velocity-gradient evolution in compressible turbulence. *J. Fluid Mech.* **683**, 289–319.

TAULBEE, D. & VAN OSDOL, J. 1991 Modeling turbulent compressible flows: the mass fluctuating velocity and squared density. *AIAA Paper* 1991–0524 (doi: http://dx.doi.org/10.2514/6.1991-524).

TSUJI, Y., FRANSSON, J. H. M., ALFREDSSON, P. H. & JOHANSSON, A. V. 2007 Pressure statistics and their scalings in high-Reynolds-number turbulent boundary-layers. *J. Fluid Mech.* **585**, 1–40.

WANG, J., SHI, Y., WANG, L.-P. & HE, X. 2011 Effect of shocklets on the velocity gradients in highly compressible isotropic turbulence. *Phys. Fluids* **23**, 125103.

WEI, L. & POLLARD, A. 2011 Interactions among pressure, density, vorticity and their gradients in compressible turbulent channel flow. *J. Fluid Mech.* **673**, 1–18.

ZHANG, Y. S., BI, W. T., HUSSAIN, F. & SHE, Z. S. 2013 A generalized Reynolds analogy for compressible wall-boundaed turbulent flows. *J. Fluid Mech.* **739**, 392–420.